Science and Technology of Advanced Materials

ISSN: (Print) (Online) Journal homepage: www.tandfonline.com/journals/tsta20

Theoretically designed M@diaza[2.2.2]cryptand complexes: the role of non-covalent interactions in promoting NLO properties of organic electrides

Atazaz Ahsin, Aamna Qamar, Qing Lu & Wensheng Bian

To cite this article: Atazaz Ahsin, Aamna Qamar, Qing Lu & Wensheng Bian (20 May 2024): Theoretically designed M@diaza[2.2.2]cryptand complexes: the role of non-covalent interactions in promoting NLO properties of organic electrides, Science and Technology of Advanced Materials, DOI: 10.1080/14686996.2024.2357064

To link to this article: https://doi.org/10.1080/14686996.2024.2357064

Publisher: Taylor & Francis & The Author(s). Published by National Institute for Materials Science in partnership with Taylor & Francis Group.

Journal: *Science and Technology of Advanced Materials*

DOI: 10.1080/14686996.2024.2357064

Theoretically designed M@diaza[2.2.2]cryptand complexes: the role of non-covalent interactions in promoting NLO properties of organic electrides

Atazaz Ahsin[1,3] Aamna Qamar[2,3] Qing Lu[1*] Wensheng Bian[1,3*]

[1]Beijing National Laboratory for Molecular Sciences, Institute of Chemistry, Chinese Academy of Sciences, Beijing 100190, China

[2]Beijing National Laboratory for Molecular Sciences, State Key Laboratory of Polymer Physics and Chemistry, Chinese Academy of Sciences, Beijing 100190, China

[3]School of Chemical Sciences, University of Chinese Academy of Sciences, Beijing 100049, China

Correspondence[*]: qinglu@iccas.ac.cn (Q. L), bian@iccas.ac.cn (W. B)

Abstract

Organic excess electron compounds with significant nonlinear optical (NLO) properties are widely employed in optoelectronic applications. Herein, single-alkali metals with diaza[2.2.2] cryptand (M@crypt,M=Li, Na, and K) are investigated for optoelectronic and NLO properties by using the density functional theory. Thermodynamic and kinetic stabilities of present complexes are computed through interaction energy (E_{int}) and *ab-initio* molecular dynamic (AIMD) simulations. M@crypt complexes carry excess electrons and mimic molecular electrides. Quantum theory of atoms in molecules (QTAIM) analysis and reduced density gradient (RDG) spectra demonstrate the roles of the weak van der Waals (vdW) interactions between metal and complexant. The remarkable hyperpolarizability (β_o) value up to 1.41×10^6 au may be credited to the presence of loosely bound excess electrons. The hyper Rayleigh scattering hyperpolarizability (β_{HRS}) is recorded up to 1.31×10^6 au for the K@crypt. Furthermore, frequency-dependent first-order and second-order hyperpolarizability is more prominent at the applied frequency of ω=0.042823 au. The electron localizing function (ELF) and localized orbital locator (LOL) analysis further disclose the nature of interaction between alkali metal and complexant. The TD-DFT method is adopted to get excited state parameters and absorbance properties. An electron density difference map (EDDM) is exploited to evaluate the orbital contributions in excited states. Hence, the studied electride may become a promising candidate for NLO materials. We anticipate that the present work will provide insight into further development of molecular electride for optoelectronic applications.

Keywords; Electrides; Excess electrons; Optoelectronic; Molecular dynamics; DFT.

Introduction

Nonlinear optical (NLO) materials have been extensively used in the fields of fibre optics, data transformation, photonic lasers, and data storage in wireless communication due to the recent advancement in optics [1][2][3]. After the discovery of the first working ruby laser by Maiman in 1960, optics became a more intense subject in interdisciplinary science [4]. Several materials have demonstrated excellent optical nonlinearity in recent decades, including organic materials [5], perovskite quantum dots [6], nanoclusters [7], and organic-inorganic hybrid materials [8][9]. Therefore, scientists are focusing on the development of novel organic NLO materials to establish future society. Numerous organic crystals, such as 4-dimethylamino-N-methyl-4-stilbazolium-tosylate (DAST) [9], N-benzyl-2-methyl-4-nitroaniline (BNA) [10], and 2,7-di(pyridine-3-yl)-9H-flupren-9-one (3-DPyFO) and 2,7-di(pyridine-4-yl)-9H-flupren-9-one (4-DPyFO), have been found to exhibit the NLO effect [10].

Asymmetric charge distribution [11], significant dipole moment (μ_o), and low excitation (ΔE) energy, are considered crucial factors in enhancing the NLO response of molecular materials [12][13]. Up till now, various kinds of measures have been considered to improve the molecular structure for promoting the optoelectronic at the molecular level. Among the adopted strategies, constructing donor-conjugated-bridge-acceptor (D-A) models [14], introducing push-pull effects [15], making sp^2-hybridized carbon-based materials [16], designing multidecker sandwiches complexes [17], creating octupolar molecules [18], bond length alternation (BLA) theory [19], and introduction of loosely bound electrons (excess electrons) are very renowned for constructing NLO materials [20][21]. Among the above-stated techniques, investigating excess electron molecules is perhaps the most fascinating way to enhance the NLO properties. The doping of transition and main group metals [on host molecules] is an emerging approach for introducing excess electrons into materials [22][23]. Research has shown that the existence of loosely bound electrons greatly reduces the

excitation energy (ΔE), facilitates electron promotion to unoccupied orbitals, and is required for regulating the optical and NLO characteristics [24][25][26].

Alkalides (alkali anion) [27], alkaline earth metals earthides [28], and electrides [23] are the main classes of excess electron compounds and were studied for various applications. In alkalides, the alkali metals act as anions (Li^-, Na^- and K^-) for charge transfer, while the 2nd group (earth metals) contains anionic nature in earthides. Theoretically designed alkalides were reported using the alkali metals and superalkali clusters with various complexant [27][29]. In such complexes, the role of alkali metal is to transfer charge, and strong polarization was seen. For instance, Ayub *et al* [29] have designed an alkalides Li_3O@[12-crown-4]M (where M=Li, Na, and K) as excess electrons complexes by simultaneous doping of Li_3O and alkali metals on the crown ether. Similarly, a variety of diffuse excess electron compounds were designed for NLO applications based on cages and crown ether complexes [30][31]. Electrides containing excess electrons (diffuse excess) in lattice voids as anions have grabbed considerable attention in both fundamental research and application development [32]. The very first evidence about the synthesis of electride was received in 1983 by Dye and co-workers. Since then, numerous organic and inorganic electrides have been reported [33][34]. Johnson and colleagues investigated eight organic electrides through a DFT study and the presence of localized interstitial electrons justifies their electrides properties [35]. They also claimed the strong adsorption affinity Na^+ through complexation with cryptand (crypt), containing eight tertiary amine nitrogen [36]. Owing to the excess electron nature of electride, they are continuously considered to construct remarkable NLO materials. Very recently, Wajid *et al* theoretically designed alkali metals doped $C_6O_6Li_6$ organometallic electrides for optical and NLO applications[37]. For the K@$C_6O_6Li_6$ complex, the hyperpolarizability (β_o) value was recorded up to 2.9×10^5 au. Likewise, M_3O@$C_6S_6Li_6$ (*M* = K, Na, Li) electrides were also reported for geometric, electronic, and optical properties [38].

Cryptands belong to the family of synthetic bi- and polycyclic organic compounds and have received great attention due to their excellent structural feature. Cryptand-based hosts are very famous for unique 3-dimensional structures, which can be exploited in constructing novel complexes [39][40]. In 1987 Lehn and their co-workers [41] successfully synthesized cryptand for the first time. The interior cavity can be operational for the sitting of guest molecules and atoms in modifying its properties. Using the cavity of benzocryptand, Nimra *et*

al have reported alkali metals doped benzocryptand for NLO application, where hyperpolarizability response was recorded up to 9.1×10^5 au [42]. The evidence of the strong interaction of alkali metal cations with cryptand and their trapped electrons (electride) has already been emphasized [43]. The Dye group has experimentally reported thermally stable K^+(cryptand 2.2.2)e^- electride, where ionic solids with cavity-trapped electrons serve as the anions [44][45].

Inspired by earlier developments in molecular electrides and their NLO properties, we theoretically designed single alkali metal-based electrides based on diazacryptand [2.2.2]. We aim to uncover the electride nature, and role of noncovalent interactions in promoting optoelectronic properties of M@crypt (where M=Li, Na, and K) complexes (Fig.1). It should be noted that the van der Waals (vdW) interaction is a kind of important noncovalent interactions, which plays very important roles in many chemical processes [46][47], and includes dispersion interaction as well as others. Its role in the formation and properties of molecular complexes is of great interest.

Computational Methodology

The ground state structures of the designed M@crypt were fully optimized with the ωB97xd/def2-tzvp level of theory. The entire simulations were performed using the Gaussian 16 and ORCA 5.0 package [48][49]. The long-range corrected method (ωB97xd) yields satisfactory results for thermochemistry, adsorption study, and non-covalent interactions [50]. Interaction energies are calculated at same method to justify the thermodynamic stability of present complexes. Additionally, we have performed *ab-initio* molecular simulation (AIMD) at 300 K to assess the kinetic and thermodynamic stability using the ORCA 5.0 program. Results of AIMD comprise 1500 distinct geometries in each trajectory of the complex, which are adopted for further analysis. Furthermore, AIMD is executed for 750 femtoseconds (fs) with a step size of 0.5 using the B3LYP-D3/def2-SVP method [44]. The adsorption nature of complexes is determined through calculated interaction energy (E_{int}), which is given by the following relation;

$$E_{int} = E(M@crypt[2.2.2]) - \{E(M) + E(crypt[2.2.2])\} \text{ (where M=Li, Na, and K)} \quad 1)$$

The charge transfer study, electride character, and orbital energies are also calculated through NBO and frontier molecular orbital (FMO) theory. Vibrational frequencies are computed using the same method, where the mode of vibrations is compared with the experimental

study. Vertical ionization potential (IP), electron affinity (EA), and hardness (η) were computed for the present complexes. These parameters are given by the following equations [51][52];

$$\text{Vertical Ionization potential (VIP)} = E_{(COMPLEX)^+} - E_{(COMPLEX)^0} \quad 2)$$

$$\text{Vertical electron affinity (EA)} = E_{(COMPLEX)^-} - E_{(COMPLEX)^0} \quad 3)$$

$$\eta = \left(\frac{\partial^2 E}{\partial N^2}\right)_{V(r)} \quad 4)$$

The optical and nonlinear optical (NLO) properties were characterized through calculated values of polarizability (α_o), hyperpolarizability (β_o), and projection of hyperpolarizability on dipole moment (β_{vec}) using the ωB97xd /def2-tzvp level of theory. A comparison of static NLO properties is made using the CAM-B3LYP and M062X, and ωB97xd method with def2-tzvp basis set. Scattering hyperpolarizability values are calculated for hyper Rayleigh scattering measurement at the ωB97xd/def2-tzvp level of theory. The effect of solvent on NLO response is also considered using the same method. Frequency-dependent (dynamic) first-order hyperpolarizability β(ω) and second-order hyperpolarizability γ(ω) were calculated at the applied frequencies of 532 and 1064 nm using ωB97xd /def2-tzvp at which frequencies experimental studies were carried out.

Perturbation theory may be used to calculate the energy and nonlinear optical parameters. The Taylor expansion describes the energy of the perturbed system.

$$E = E^O - \mu_I F_i - \left[\frac{1}{2!}\right]\alpha_{ij}F_iF_j - \left[\frac{1}{3!}\right]\beta_{ijk}F_iF_jF_k - \left[\frac{1}{4!}\right]\gamma_{ijkl}F_iF_jF_kF_l \quad 5)$$

$$\mu = \sqrt{{\mu^2}_X + {\mu^2}_Y + {\mu^2}_Z} \quad 6)$$

$$\alpha_{ij} = \left(\frac{\delta\mu_i}{\delta F_j}\right)_{E\to 0}$$

$$\alpha_{tot} = \frac{1}{3}(\alpha_{xx} + \alpha_{yy} + \alpha_{zz}) \quad 7)$$

The magnitude of hyperpolarizability can be defined as;

$$\beta_x = \beta_{xxx} + \beta_{xyy} + \beta_{xzz}$$

$$\beta_y = \beta_{yyy} + \beta_{yxx} + \beta_{yzz}$$

$$\beta_x = \beta_{zzz} + \beta_{zxx} + \beta_{zyy}$$

$$\beta_{tot} = \sqrt{\beta^2{}_x + \beta^2{}_y + \beta^2{}_z} \quad 8)$$

$$\gamma = \gamma_{tot} = \frac{1}{5}(\gamma_{xxxx} + \gamma_{yyyy} + \gamma_{zzzz} + 2\gamma_{xxyy} + 2\gamma_{xxzz} + 2\gamma_{yyzz}) \quad 9)$$

Hyper-Rayleigh scattering (β_{HRS}) response is described as [53];

$$\beta_{HRS}(0;0,0) = \sqrt{\{(\beta_{ZZZ}{}^2)\} + \{(\beta_{ZXX}{}^2)\}} \quad 10)$$

The β_{HRS} is composed of dipolar $\varphi(\beta_{J=1})$ and octupolar $\varphi(\beta_{J=3})$ contribution to total hyperpolarizability and given by [54];

$$\langle\beta_{ZZZ}{}^2\rangle = \frac{9}{5}|\beta_{J=1}|^2 + \frac{6}{105}|\beta_{J=3}|^2$$

$$\langle\beta_{ZXX}{}^2\rangle = \frac{1}{45}|\beta_{J=1}|^2 + \frac{4}{105}|\beta_{J=3}|^2 \quad 11)$$

To unfold the nature of the interaction between metal and crypt, topology analysis was exploited using Bader's quantum theory of atoms in molecules (QTAIM) and reduced density gradient (RDG) spectra [55]. In this analysis, we considered bond critical points (BCP) at (3,-1) electron density. Electron density difference maps are also obtained with the same method. An excited state analysis was carried out using TD-ωB97xd/def2-tzvp to get the absorbance pattern, excitation energy, and orbital contributions during the crucial transition. The projected density of states (PDOS) spectra were plotted using GaussSum and multiwfn software [56]. In addition, the electron localizing function (ELF) and localized orbital locator (LOL) are plotted to understand the bonding properties in present complexes. The kinetic energy density plays a vital role in the description of a chemical bond, since the driving force in forming a covalent bond. The ELF function can nicely unveil the location of atomic shells, core binding electrons, and lone pairs electrons in atomic and molecular orbitals. Mathematically, the ELF can be expressed based on kinetic-energy density [57];

$$\text{ELF} = (1 + x^2{}_\sigma)^{-1} \quad 12)$$

$$\text{Where}\chi_\sigma = \frac{D_\sigma}{D_\sigma{}^0} \text{ and } D_\sigma{}^0 = \frac{5}{3}(6\pi^2)^{2/3}\rho_\sigma{}^{5/3} \quad 13)$$

Where D_{σ^0} is uniform electron gas with a spin density equal to the local value of ρ_σ (r) χ_σ ratio is a dimensionless quantity, indicating localization index and calibrated by considering uniform-density electron gas as reference.

$$0 \leq \text{ELF} \leq 1 \qquad 14)$$

The possible ELF values range with the upper limit ELF=1, indicating perfect localization and the value of ELF= 0.5 represents the electron gas-like pair probability.

On the other hand, the LOL is similar to the ELF, where just the orbital kinetic energy density and the local spin density approximation (LSDA) kinetic energy density are compared, without considering the Pauli repulsion [58]:

$$LOL_\sigma = \frac{1}{1+\frac{2t_\sigma}{t_\sigma{}^{LSDA}}} \qquad 15)$$

Results and Discussion

Electronic structure and energetic analysis of complexes

The optimized geometries of M@crypt (M=Li, Na, K, and crypt = diazacryptand[2.2.2]) complexes using ωB97xd/def2tzvp are shown in Figure 1. The adsorbed alkali metals have unequal interaction distances from bridgehead nitrogen atoms ($d_{M\text{-}N}$) and with the oxygen of the cyclic ring ($d_{M\text{-}O}$). The interaction of alkali metals with nitrogen and oxygen is crucial to characterize the physico-chemical properties of complexes. Only influential bond distances were computed and values are given in supplementary information (Table S1). In a reported study on the same system, the geometries of K@crypt and Na@crypt complexes were slightly distorted from the ideal D_3-group [59]. In the present results, a similar scenario is seen except for a slight distortion in Li@crypt, where Li is asymmetrically adsorbed in the cavity. In Li@crypt, the calculated bond distances between Li63-N7 and Li63-N8 are 3.95 and 2.46 Å. The Li-atom has a higher distance with N7 while strongly interacting with lower bridgehead nitrogen (N8). Similarly, average optimized distance of Li-atom with oxygen ($d_{M\text{-}O}$) is 2.34 to 2.70 Å. For Na@crypt, the interaction distance between the Na1-N8/N9 is 3.19 Å (Table S1). Similarly, Na1 is equidistant from O4/O5 calculated up to 2.48 Å. The interaction distance of K63- N7 and K63-N8 is 3.07 Å

(see Table S1). K-metal is adsorbed exactly in the middle of the cavity and is equidistant from nitrogen (N7, and N8) and oxygen of the ring. The obtained structural results were also compared with the reported experimental synthesis of (2.2.2-cryptand)potassium nitrate hydrate complex [60], and values are given in supplementary information (Table S1). The K-O interaction distance reported by Boldyrev et al [59] has a comparable value to the present results (see Table S1). There is no imaginary frequency associated with complexes, denoting their stability on potential energy surfaces.

The obtained significant interaction energies (E_{int}) quantify their thermodynamic stability (see Table 1). The interaction energies range from -11.10 to -21.91 kcal/mol, where the highest value is obtained for Li@crypt, while the lowest is calculated for Na@crypt. Overall, the E_{int} of present electrides are higher in comparison with the reported electride, evidencing the strong interaction and formation of stable complexes. The significant E_{int} of Li@crypt is in accordance with the least interaction distances of Li with N7 (2.46 Å) and oxygen atoms (2.70 Å). The E_{int} (-21.91 kcal/mol) of present Na@crypt is higher than alkali-doped benzocryptand [42], superalkalis doped all-cis-1,2,3,4,5,6-hexachlorocyclohexane [61], and $M_3O@C_6S_6Li_6$ (*M* = K, Na, Li) electrides.

A comparison of the vibrational study of the pure complexant (diazacryptand) and alkali metal-encapsulated complexes is made with reported FT-IR analysis to monitor changes in vibrational modes. The vibrational frequency and their comparison with the experimental values are summarized in supplementary information (Table S2). For the crypt, the intense peaks of C-H stretching vibrations were observed in the range of 2812 to 2981 cm^{-1}. C-H bending peaks range from 1280 to 1523 cm^{-1} and are second-strong peaks. The experimental value of C-H stretching ranges from 2790 cm^{-1} to 2877 cm^{-1} (see Table S2) [62]. Further details of characteristics IR peaks is given in supplementary information (see section S2)

Ab-initio molecular dynamics (AIMD) calculations of designed complexes were performed using ORCA 5.0.2, time step 0.5 (fs), and at room temperature (300 K). AIMD results show that M@crypt remained stable during simulation, with rigid structures against isomerization and decomposition. The root-mean-square deviation (RMSD) for complexes

and pure crypt is plotted and given in supplementary information (see Figure S1). RMSD is a standard measure of structural distance between coordinates. The variation in kinetic energy versus time is also plotted in Figure S1b. In the beginning, kinetic energy increases for complexes up to 200 fs while equilibrium is attained after 300 fs. Additionally, the drift energy (K) versus time (fs) spectra were also given in supplementary information (Figure S2). The drift energy (K) of Li@crypt is higher in the beginning and near 800 fs. Likewise, the drift energy for Na@crypt is maximum near 200 fs and noticeably reduced at 700 fs. The snapshots of geometries after 100 fs are captured to ensure the rigidity of complexes against dissociation and are shown in the supplementary information (Figure S3). The curves of complexes have an uptrend with the increased size of metals (Li to K). Hence, the AIMD study reveals their thermodynamic and kinetic stability at room temperature.

The computed partial NBO charges are given in Table 1. The calculated charges on alkali metals Q(M) are slightly positive and range from 0.40 to -0.0001 |e|. In Li@crypt, the small Li to nitrogen distance (d_{M-N}) causes significant charge transfer (due to strong interaction) to nitrogen (N7), which ranges from -0.65 to -0.57 |e|. Similarly, for the Na@crypt complex, slightly reduced NBO charge (positive) on Na-atom up to +0.013 |e| while, the K-atom shows negligible positive NBO charge. Due to the interaction of metals with cryptand, ns^1 electrons are polarized by neighbour atoms (N and O) of complexant. The lowest polarization of partial charge is observed on the K-atom, attributing to symmetric adsorption of K-metal inside cavity. One can conclude that loosely bound electrons are trapped inside the complexant and induce the electride nature to complexes. The electride nature and charge transfer predominately enhance the optical properties, which will be shown later. Further justification of electride nature and orbital energies can be established through frontier molecular orbital (FMO) analysis (see section S3). The orbital shapes of present complexes are given in Figure 2. The HOMO is not warping a particular atom distributed in space in the complexant. After the alkali-metals encapsulation, these complexes have HOMO and LUMO in space distributed within the entire complexant, which is reminiscent of the molecular electride. The HOMO has diffused shape and indicates excess electrons are trapped inside the complex. Vertical ionization potential (VIP), electron affinity (VEA), and chemical hardness (η) are also calculated and values are given in Table 1. The VIP of the pristine crypt is 7.56 eV, while its VEA is 3.14 eV. After the interaction of alkali metals (Li, Na, and K), a significant reduction in VIP and VEA values is observed. The calculated VIP values of complexes are 1.90, 1.01, and 1.08 eV for Li@crypt, Na@crypt, and K@crypt,

respectively. VIP values are endowed to be useful to manifest their capability to donate and accept electrons. The reduced VIP values with increased alkali metals size (Li to K) suggest the electropositivity and excellent reducing ability of present complexes. Smaller ionization potential than Cs-atom (3.87 eV) also suggests their superalkali-like nature [63]**.** The VIP, VEA, HOMO-LUMO gaps, and interaction energies are compared with similar reported complexes and values are given supplementary information (Table S3).

Static nonlinear optical (NLO) properties of complexes

Owing to the electride nature of present complexes, one may envisage interesting NLO features. Various excess electron compounds were investigated as efficient NLO candidates, in which electrides are the most promising candidates [64][65][22][66][26][67]. NLO parameters of M@crypt (electrides) are given in Table 2. The dipole moment (μ_o) plays a vital role in studying the polarization, packing, and asymmetric charge distribution. A notable value of μ_o can be correlated to higher NBO charges on and asymmetric interaction between metal (M) and cryptand. A remarkable μ_o of Na@crypt complex may be credited to the strong asymmetric interaction of metal Na1 with N7, N8, and oxygen atoms of the cryptand ring. The lowest value of μ_o can be seen in K@crypt, where K63 is exactly in the middle of the cryptand cavity. Static polarizability (α_o) provides information on the distribution of electrons in a molecule and is critical in deciding the polar nature and reactivity of present complexes. The obtained (α_o) value of pristine complexant is 2.54×10^2 au, while after the interaction of alkali metals M@crypt, the α_o increased up to 9.30×10^2 au (Table 2). Also, the z-component shows a significant contribution to the total polarizability response. The gradual increase in α_o is observed as follows: K@crypt >Li@crypt > Na@crypt. The values of α_o at M06-2X/def2qzvp and CAM-B3LYP/def2tzvp method are close to ωB97xd with same basis set and are provided in supplementary information (Table S4).

On the other hand, the hyperpolarizability (β_o) values of complexes are 5.32×10^3, 1.41×10^6, and 9.30×10^5 au for Li@crypt, Na@crypt, and K@crypt, respectively, where the highest value is observed for the Na@crypt complex (Table 2). The calculated significant value of 1.41×10^6 is higher than that of the organic reference molecule (P-nitroaniline). Likewise, the computed β_o value of 1.41×10^6 au for Na@crypt is quite higher than those of previously reported $M@C_6O_6Li_6$ electrides, superalkali@$Al_{12}P_{12}$ electrides [37][68]. The

non-monotonic trend of β_o for the Na@crypt complex using ωB97xd/def2tzvp might be attributed to its high dipole moment and low excitation energy (1.22 eV). Also, the asymmetric interaction has significantly altered the β_o response in Na@crypt. The β_o response of designed electrides can be correlated to electronic properties like VIP, EA, and chemical hardness. In the current study, lower VIP values indicate an increased β_o response. For instance, the highest β_o value of Na@crypt has the lowest VIP value (1.0), followed by K@crypt, where the VIP value (1.08 eV) is slightly higher using ωB97xd/def2-tzvp. A similar trend in values of projection of hyperpolarizability on dipole moment vector (β_{vec}) and total hyperpolarizability (β_o) can be seen which indicates excellent nonlinear optical properties of present complexes. The static second-order hyperpolarizability (γ_o) is considered to be an important index to measure nonlinear optical coefficients of designed electrides. These values are calculated using ωB7XD/def2-tzvp and given in Table 3. The γ_o values are 1.05×10^4, 4.30×10^5, 2.96×10^8, and 4.96×10^9 au, respectively for crypt, Li@crypt, Na@crypt, and K@crypt. A gradual increase in γ_o can be seen with increased size of alkali metals (see Table 3). In contrary to hyperpolarizability, γ_o responses exhibit a dependence on the size of alkali metals. The obtained significant γ_o value of 4.96×10^9 au for K@crypt is quite higher than previously reported alkali metal doped $C_6O_6Li_6$ organometallics electride, superalkalis doped $C_6O_6Li_6$ electrides [69], superalkalis@$Al_{12}P_{12}$ inorganic electrides [68], and alkaline-earth-based alkaline salt electrides M-$H_3C_4N_2$···Ca (M=H, Li, and K) [70]. Observed β_o and γ_o values of M@crypt were significantly higher as compared to alkali and alkaline earth metal-based benzocryptand, superalkali@$C_6F_6H_6$ electride, and Li_3@C_{60} electride. Table S4 reveal the comparable β_o values at M062X and ωB97xd method, while values at CAM-B3LYP are slightly declined. A comparison of NLO parameters of present complexes is also made with reported similar molecular electrides and excess electron compounds using the ωB97xd method (Table S5).

The hyper-Rayleigh scattering (HRS) first-order hyperpolarizability (β_{HRS}) of pure cryptand and electride complexes is also calculated using the same method. β_{HRS} is the most fundamental nonlinear chiral optical (chiroptical) effect to characterize the nonlinearity of molecular materials even with zero dipole moment. β_{HRS} is an important theoretical tool to measure the hyperpolarizability of centrosymmetric molecules [71]. The calculated values of β_{HRS}, depolarization ratio (DR), dipolar contribution to hyperpolarizability (DR), percentage of dipolar contribution Φβ(j=1) and octupolar contribution to total hyperpolarizability Φβ(j=3) are given in Table 3. The undoped crypt holds a very low HRS (170.21) response as

compared to M@crypt. For M@crypt, obtained β_{HRS} values are 1.33×10^4, 9.0×10^5, and 1.31×10^6 au for Li@crypt, Na@crypt, and K@crypt, respectively. K@crypt is more responsive to HRS measurement, which can be correlated to the size of metal. The higher depolarization ratio (DR) indicates the dipolar nature of complexes. Pristine (crypt) shows the lowest DR ratio justifying its octupolar nature. The octupolar nature of the crypt is seen in its 99% contribution to hyperpolarizability at Φβ(j=3). Complexes with a high percentage contribution from dipolar factor are characterized as dipolar (*vide supra*). The dipolar contribution to hyperpolarizability Φβ(j=1) is almost 52% for Li@crypt, while Na@crypt and K@crypt complexes are octupolar due to significant contribution from Φβ(j =3).

Frequency-dependent (dynamic) NLO properties

The frequency-dependent hyperpolarizability β(ω) is calculated as β(-ω,ω,0) for electro-optical Pockel's effect (EOPE) and β(-2ω, ω, ω) for second harmonic generation phenomena (SHG) parameter. Entire frequency-dependent NLO parameters are given in Table 4. To investigate the frequency-dependent NLO responses of the current complexes, we chose 532 and 1064 nm as transparent regions since the complexes display significant absorbance in between 700 to 1016 nm. The choice of wavelength (1064 nm) is also relevant to Nd:YAG laser functioning, which frequently emits invisible light in 1064 nm and serves in laser-based devices [72]. The electro-optic effect is the modification of a medium's refractive index produced by an electric field. The electro-optical effect (Pockels effect) is an essential nonlinear effect used in many applications [73]. Only non-centrosymmetric materials (mostly nonlinear crystal materials) show the linear electro-optic effect, also known as the Pockels effect, in which the change in refractive index is proportional to the strength of the electric field. Overall, EOPE values are higher than those of electric field-induced second harmonic generation (ESHG) values at both frequencies. The EOPE values are 7.99×10^3, 1.34×10^4, 1.11×10^5 au respectively for Li@crypt, Na@crypt, and K@crypt at larger frequency (ω=0.085645). EOPE effect is most prominent at both frequencies. The highest value (9.55×10^7 au) of EOPE is calculated for Na@crypt complex. The frequency-doubling nonlinear optical process is determined through ESHG. The ESHG values are almost comparable at both frequencies, while significantly lowered than those of EOPE. Frequency-dependent second-order hyperpolarizability γ(ω) is estimated using γ(-ω, ω,0,0) for dc-Kerr effect and γ(-2ω,ω,ω,0) as second harmonic generation phenomena (SHG). The computed parameters are given in Table 4. The Kerr effect, also known as the quadratic electro-optic (QEO) effect, is a change in a material's refractive index in response to an applied electric

field. The Kerr effect (electro-optic effect) reveals the nonlinear change in the refractive index of materials after externally applied fields. The nonlinear refractive index is given as [74];

$$\Delta n = \lambda K E^2$$

16

where γ, K, and E are the wavelength of light, Kerr constant, and electric field strength, respectively. One can observe the higher Kerr effect takes place at a smaller frequency dispersion (ω=0.042823 au). At 1064 nm, the highest dc-Kerr value of 7.36×10^{12} au is recorded for Na@crypt, while lowest is while lowest is Li@crypt (Table 4). The higher value of the Kerr effect also demonstrates a larger change in the refractive index of studied complexes. Overall, at both frequencies, the dc-Kerr γ(-ω, ω,0,0) beats SHG response.

Role of non-covalent interactions in promoting NLO responses

Quantum theory of atoms in molecules (QTAIM) has been exploited to identify the bonding nature in M@crypt complexes. The presence of van der Waals (vdW) forces and other interactions are recognized as additional influencing factors in describing NLO properties of present complexes. Additionally, noncovalent interactions have crucial roles in describing chemical events and the stability of complexes in various organometallic and biological processes [75][76][77][78][79][80][81]. For the present complexes, we considered only bond critical points (BCP) using (3, -1) especially for the interactions zone to elucidate the nature and strength of attractive interactions. In Li@crypt, the Li63 atom shows interaction with O6/O4 and N8 atoms, while Na1 and K63 interact with oxygen (O1, O2, O3, O4, O5, and O6) atoms of cryptand only. Labeled structures with critical points and atoms are given in Figure 3a, while their corresponding parameters from CP are given in supplementary information (Table S6). Generally, greater values of electronic density (ρ_r) > 0.1 and negative Laplacian of electronic density (∇^2_ρ) indicate strong interactions like hydrogen bonding and electrostatic interactions. In contrast, the smaller value of ρ_r and positive ∇^2_ρ represents the presence of vdW interactions. The ∇^2_ρ has a positive value for entire interactions involving

Li63 with nitrogen and oxygen atoms. Also, ρ_r is reduced and becomes less than 0.1, rationalizing the non-covalent nature of the interaction of Li63 inside the cavity. BCP 146 and 107 depict the N7—C54 and O4—C21 interactions having negative values for ∇^2_ρ, which disclose the presence of strong interaction (covalent bond). The ∇^2_ρ and energy density (H_r) values at BCP (3, -1) for Li63 interaction with N8, O1, O4, O6, and O4 are positive, indicating the non-covalent nature of bonding between atoms. Similarly, ∇^2_ρ and H_r at BCP (3, -1) are positive for Na1 interactions with O2, O4, O5, O6, and O7 pointing to its weak bonding. Na@crypt where Na1---O6/O7/04/O2/O5 has weak noncovalent interactions with complexant (crypt). For K63---O1, a small value of total electronic density (0.0127 au) is observed. Likewise, total electronic density values are also small for K63-O2, K63-O3, K63-O4, and K63-O5 interactions, justifying the presence of weak interactions or vdW forces. The values of ρ_r are less than 0.1 au, and positive values of ∇^2_ρ rationalize the presence of non-covalent interaction. The BCP for N7—K63 and N8---K63 also unfold the weak interaction (noncovalent) from the value of their electronic density and ∇^2_ρ. On the other hand, the BCP (98) shows the O2---C36 bond, which has negative ∇^2_ρ, while ρ_r is higher than 0.2, indicating strong interactions (covalent bond). Figure 3b displays the reduced density gradient (RDG) scatter graph, where the λ_2 sign is exploited to differentiate between the bonded ($\lambda_2<0$) and non-bonded ($\lambda_2>0$) interactions. RDG scatter plots with colour-graded depict the type of interactions between alkali metals and cryptand, where the strong attraction (blue), the weak interaction (green), and the strong repulsion (red) are shown in spikes ranging from -0.035 to +0.020 au. The blue color side of Figure 3b indicates strong inductive or attractive interactions. One can observe an increase in vdW forces due to interactions between metal (M=Li, Na, and K) and cryptand. The vdW interactions are more prominent in Li@crypt and Na@crypt, which agrees with the previous analysis. Therefore, the existence of noncovalent interaction between M—O/M—N may have a significant impact on triggering the complexes' optical and NLO response.

Electron localized function (ELF) and localized orbital locator (LOL) are shown in Figure 4. ELF map is designed in the range of 0.0 to 1.0; however, the delocalized electronic region falls below 0.5. The covalent region (electron-rich) shows high electron density in space where electrons are localized. From the results of color filled ELF map, the red-colored regions of the diaza cryptand [2.2.2] are observed for the hydrogen of the group. Generally, the higher ELF and LOL values, significant localization of electrons, which may be responsible for the existence of covalent bonds, inner shells, or a lone pair of electrons. The

synaptic nature of the non-bonding lone pair of electrons on oxygen atoms with alkali metals in M@crypt is displayed in blue color regions in the ELF and LOL map [82]. In the Li@crypt, Li63 has a high ELF value (red region) which indicates that ns^1 is not completely ionized and still bound with its valence. However, due to the strong interaction of Li63 to the lower side of the crypt, a significant increase in ELF value (red color) can be observed for N8, C12, C18, C15, and hydrogen atoms (H28, 25, 13, and 16). For Na@crypt, ELF value is decreased for Na1, which reveals the ns^1 valence electrons are more delocalized to ring in composing a diffuse excess electrons model. Na1 is separated by a blue color region, displaying its non-covalent interaction with O2, O4, O5, O6, and O7. In the K@crypt complex, K63 shows further reduced ELF value, while the CH_2-group hold strong localization (red region). The valence electrons of K are diffused to the entire ring composing an anionic interstitial in cryptand. The Blue color shade can be seen in the LOL spectra of complexes, indicating the delocalized nature of electrons in complexes. The existence of blue circles around the alkali metals unveils the electron deficiency, transferring to complexant (crypt). Mathematically, ELF and LOL exhibit similar chemical mapping because they depend on the kinetic energy density. The ELF function can nicely unveil the location of atomic shells, core binding electrons, and lone pairs electrons in atomic and molecular orbitals. It is a dimensionless quantity, in the range of 0–1, to provide a visual description of the chemical bond for present complexes. Furthermore, ELF includes the Pauli kinetic energy density, while the LOL analysis does not include Pauli repulsion. Mathematically, the ELF can be expressed based on kinetic energy density. In contrast, the increased delocalization of electrons can be observed from Li@crypt to K@crypt. Moreover, the neutral region on LOL (light green) can be seen on bridgehead nitrogen atoms of aza-cryptand, while methylene (CH_2) moieties of cryptand indicate higher delocalization of electrons.

UV-visible study

For the designed M@crypt complexes, UV-Vis spectral study is exploited using the TD-DFT/ωB97xd/def2tzvp method. In this analysis, the absorbance wavelength (λ), excitation energy (ΔE), and oscillator strength (O.S.) are determined. The contribution of major orbitals during the excitation from HOMO-LUMO is very crucial in the NLO study. Out of 40 excited states, we considered only the crucial state (with significant oscillator strength) for obtaining the excited state parameters (see Table 5). The pure cryptand shows absorbance in the deep ultraviolet region while after complexation with alkali metals, a dramatic increase in

absorbance wavelength (bathochromic shift) is seen (see Figure 5). The highest absorbance maxima (λ_{max}) is accounted for Na@crypt complex at 1016 nm. Due to an appreciable reduction in excitation energy (ΔE) of Na@crypt, a vital excitation is observed from HOMO→LUMO with a contribution of 43.8%. The increased absorbance maxima can be strongly correlated to the increased atomic number of metals (M). Also, the smaller the excitation energy higher the hyperpolarizability response (vide supra). The oscillator strength (O.S.) of Na@crypt and K@crypt is higher as compared to Li@complex.

Conclusion

In summary, we have presented the optical, and NLO properties of designed complexes M@crypt based upon various quantum chemical calculations as well as the non-covalent interactions between the metal center and the cryptand. The designed complexes are similar to molecular electride and could be grouped in the excess electron family. AIMD simulations further confirm their kinetic and thermal stabilities at room temperature. The electronic structure calculations unveil their nature reminiscent of excess electron compounds, where the HOMO-LUMO gap was significantly reduced to 0.38 eV or lower. The C-N and C-O stretching vibrations become more intense after metal coordinating at the cavity of the cryptand. The remarkable value (1.41×10^6 au) of the first-order hyperpolarizability (β_o) is recorded for Na@crypt electride using ωB97xd/def2-tzvp. The β_{HRS} is recorded up to 2.5×10^7 au. The highest static second-order hyperpolarizability γ_o value of 4.96×10^9 au is calculated for K@crypt. γ_o increases gradually with the size of alkali metals. Furthermore, the frequency-dependent NLO properties are more responsive than those of static properties. Calculated NLO responses are almost identical regardless of DFT methods. The obtained results are compared to previously reported molecular electride and excess electron compounds. Increasing hyperpolarizability can be affiliated with strong van der Waals interactions, confirmed by QTAIM and RDG analyses. Electron density difference maps are employed to predict the charge transfer and distribution of electronic density after the de-

excitation of electrons. The ELF and LOL analysis further disclose the nature of chemical bonds between alkali and complexant. TD-DFT calculations reveal the excited state parameters and absorbance properties. Hence, the examined electrides (as excess electrons compounds) could be a novel addition to optical materials.

Acknowledgement
The authors acknowledge the support of the National Natural Science Foundation of China and the Beijing National Laboratory for Molecular Sciences. Additionally, A.A acknowledges the support of the Alliance of International Science Organizations (ANSO).

Conflict of interest

The authors declare that the research was conducted in the absence of any commercial or financial relationships that could be construed as a potential conflict of interest.

Data availability statement

The author confirms that data supporting the findings current study are available within the article and in its supporting information. Raw data that supports the findings of this study are available from the corresponding, upon reasonable request.

References

[1] M. Anis, G.G. Muley, A. Hakeem, et al. Exploring the influence of carboxylic acids on nonlinear optical (NLO) and dielectric properties of KDP crystal for applications of NLO facilitated photonic devices, Opt. Mater. 2015; 46:517–521.

[2] J. Wu, J. Luo, A.K.-Y. Jen, High-performance organic second-and third-order nonlinear optical materials for ultrafast information processing, J. Mater. Chem. C. 2020; 8: 15009–15026.

[3] X. Luo, Z. Li, Y. Guo, et al. Recent Progress on New Infrared Nonlinear Optical Materials with Application Prospect, J. Solid State Chem. 2019; 270: 674-685.

[4] T.H. Maiman, Stimulated optical radiation in ruby, Nature. 1960; 187: 493–494.

[5] S. Gauvin, J. Zyss, Growth of organic crystalline thin films, their optical characterization and application to non-linear optics, J. Cryst. Growth. 1996; 166: 507–527.

[6] U. e Kalsoom, R. Yi, J. Qu, et al. Nonlinear Optical Properties of CdSe and CdTe Core-Shell Quantum Dots and Their Applications, Front. Phys. 2021; 9; 612070.

[7] L.-Y. Wang, B.-Y. Shi, C.-B. Yao, et al. Size and Morphology Modulation in ZnO

Nanostructures for Nonlinear Optical Applications: A Review, ACS Appl. Nano Mater. 2023; 6: 9975–10014.

[8] H.-Y. Shen, L. He, P.-P. Shi, et al. Lead-free organic–inorganic hybrid semiconductors and NLO switches tuned by dimensional design, J. Mater. Chem. C. 2021: 9 4338–4343.

[9] T. Notake, M. Takeda, S. Okada, et al. Characterization of all second-order nonlinear-optical coefficients of organic N-benzyl-2-methyl-4-nitroaniline crystal, Sci. Rep. 2019; 9: 14853.

[10] Y. Zheng, P. Cheng, X. Qian, et al. Self-assembled organic nonlinear optical crystals based on pyridine derived fluorenone, Mater. Chem. Front. 2023; 7: 698–704.

[11] B.B. Ivanova, M. Spiteller, Noncentrosymmetric Crystals with Marked Nonlinear Optical Properties, J. Phys. Chem. A. 2010; 114: 5099–5103.

[12] X. Jiang, S. Zhao, Z. Lin, et al. The role of dipole moment in determining the nonlinear optical behavior of materials: ab initio studies on quaternary molybdenum tellurite crystals, J. Mater. Chem. C. 2014; 2: 530–537.

[13] V.M. Geskin, C. Lambert, J.L. Bredas, Origin of High Second- and Third-Order Nonlinear Optical Response in Ammonio/Borato Diphenylpolyene Zwitterions: The Remarkable Role of Polarized Aromatic Groups, J. Am. Chem. Soc. 2003; 125: 15651.

[14] A.K. Jeewandara, K.M.N. de Silva, Are Donor-Acceptor Self Organised Aromatic Systems NLO (Non-linear Optical) Active, J. Mol. Struct. THEOCHEM. 2004; 686 131.

[15] Z.B. Liu, Z.J. Zhou, Y. Li, et al. Push–Pull Electron Effects of the Complexant in a Li Atom Doped Molecule with Electride Character: A New Strategy to Enhance the First Hyperpolarizability, Phys. Chem. Chem. Phys. 2010; 12: 10562.

[16] S. Wang, Y. Dong, C. He, et al. The role of sp2/sp3 hybrid carbon regulation in the nonlinear optical properties of graphene oxide materials, RSC Adv. 2017: 7: 53643–53652.

[17] S.J. Wang, Y.F. Wang, C. Cai, Multidecker sandwich complexes $VnBenn^{+1}$ (n = 1, 2, 3) as stronger electron donor relative to ferrocene for designing high-performance organometallic second-order nlo chromophores: Evident layer effect on the first hyperpolarizability and two-dimensional N, J. Phys. Chem. C. 2015; 119: 5589–5595.

[18] O. Maury, H. Le Bozec, Molecular engineering of octupolar NLO molecules and materials based on bipyridyl metal complexes, Acc. Chem. Res. 2005; 38: 691–704.

[19] N.A. Murugan, J. Kongsted, Z. Rinkevicius, et al. Breakdown of the first hyperpolarizability/bond-length alternation parameter relationship, Proc. Natl. Acad. Sci. U. S. A. 2010; 107: 16453–16458.

[20] E. Shakerzadeh, E. Tahmasebi, M. Solimannejad, et al. Tuning the electronic-optical properties of porphyrin-like porous $C_{24}N_{24}$ fullerene with $(Li_3O)n$ = (1–5) decoration. A computational study, Appl. Organomet. Chem. 2019; 33: 1–9.

[21] A. Ahsin, K. Ayub, Oxacarbon superalkali $C_3X_3Y_3$ (X = O, S and Y = Li, Na, K) clusters as excess electron compounds for remarkable static and dynamic NLO response, J. Mol. Graph. Model. 2021; 106:107922.

[22] A. Ahsin, A. Ali, K. Ayub, Alkaline earth metals serving as source of excess electron for alkaline earth metals to impart large second and third order nonlinear optical response; a DFT study, J. Mol. Graph. Model. 2020;101: 107759.

[23] H.M. He, Y. Li, W.M. Sun, et al. All-metal electride molecules CuAg@Ca7M (M = Be, Mg, and Ca) with multi-excess electrons and all-metal polyanions: Molecular structures and bonding modes as well as large infrared nonlinear optical responses, Dalt. Trans. 2016; 45: 2656–2665.

[24] R.-L. Zhong, H.-L. Xu, Z.-R. Li, et al. Role of Excess Electrons in Nonlinear Optical Response, J. Phys. Chem. Lett. 2015; 6: 612–619.

[25] H. Maqbool, A. Rafique, I.A. Bhatti,et al. Novel endohedrally and exohedrally metals (Li, Na, and K, Ag) doped (15-crown-5) with remarkable electronic, static and dynamic NLO response, Optik. 2022; 271: 170169.

[26] A. Ahsin, A. Ali, K. Ayub, Transition metals based metalides TM-Janus-TM (where TM=Sc–Zn and Janus=$F_6C_6H_6$); A theoretical study of nonconventional metalides with excellent static and dynamic nonlinear optical properties, Mater. Sci. Semicond. Process. 2023; 162:107506.

[27] W.M. Sun, B.L. Ni, D. Wu, et al. Designing Alkalides with Considerable Nonlinear Optical Responses and High Stability Based on the Facially Polarized Janus all-cis-1,2,3,4,5,6-Hexafluorocyclohexane, Organometallics. 2017; 36: 3352–3359.

[28] A. Ahsan, K. Ayub, Extremely large nonlinear optical response and excellent electronic stability of true alkaline earthides based on hexaammine complexant, J. Mol. Liq. 2020; 297: 111899.

[29] A. Ahsin, K. Ayub, Superalkali-based alkalides Li_3O@[12-crown-4]M (where M= Li, Na, and K) with remarkable static and dynamic NLO properties; A DFT study, Mater. Sci. Semicond. Process. 2022; 138: 106254.

[30] A. Ahsan, K. Ayub, Adamanzane based alkaline earthides with excellent nonlinear optical response and ultraviolet transparency, Opt. Laser Technol. 2020; 129: 106298.

[31] L. Zhu, K. Xue, J. Hou, A theoretical study of alkaline-earthides $Li(NH_3)_4M$(M= Be, Mg, Ca) with large first hyperpolarizability, J. Mol. Model. 2019;V: 150.

[32] Z. Li, J. Yang, J.G. Hou, et al. Inorganic electride: theoretical study on structural and electronic properties, J. Am. Chem. Soc. 2003; 125: 6050–6051.

[33] F. Khaliq, T. Mahmood, K. Ayub,et al. Exploring Li4N and Li4O superalkalis as efficient dopants for the Al12N12 nanocage to design high performance nonlinear optical materials with high thermodynamic stability, Polyhedron. 2021; 200: 115145.

[34] Q. Hu, R. Tan, J. Li, et al. Highly conductive $C_{12}A_7e^-$ electride nanoparticles as an electron donor type promoter to P25 for enhancing photocatalytic hydrogen evolution, J. Phys. Chem. Solids. 2021; 149:109810.

[35] S.G. Dale, A. Otero-de-la-Roza, E.R. Johnson, Density-Functional Description of Electrides, Phys. Chem. Chem. Phys. 2014; 16:14584.

[36] M.Y. Redko, J.E. Jackson, R.H. Huang, et al. Design and Synthesis of a Thermally Stable Organic Electride, J. Am. Chem. Soc. 2005; 127: 12416–12422.

[37] S. Wajid, N. Kosar, F. Ullah, et al. Demonstrating the potential of alkali metal-doped cyclic $C_6O_6Li_6$ organometallics as electrides and high-performance NLO materials, ACS Omega. 2021; 6: 29852–29861.

[38] N. Kosar, L. Zari, K. Ayub, et al. Static, dynamic nonlinear optical (NLO) response and electride characteristics of superalkalis doped star like $C_6S_6Li_6$, Surfaces and Interfaces. 202; 31: 102044.

[39] I.S. Taschner, T.L. Walker, B.R. Schrage, et al. Topomeric aza/thia cryptands: synthesis and theoretical aspects of in/out isomerism using n-alkyl bridging, Org. Chem. Front. 2020; 7: 1164–1176.

[40] Y. Han, Y. Jiang, C.-F. Chen, Cryptand-based hosts for organic guests, Tetrahedron. 2015; 71: 503–522..

[41] B. Dietrich, J.M. Lehn, J.P. Sauvage, Diaza-polyoxa-macrocycles et macrobicycles, Tetrahedron Lett. 1969; 10: 2885–2888.

[42] N. Maqsood, A. Asif, K. Ayub, et al. DFT study of alkali and alkaline earth metal-doped benzocryptand with remarkable NLO properties, RSC Adv. 2022; 12: 16029–16045.

[43] R.H. Huang, M.K. Faber, K.J. Moeggenborg, et al. Structure of K^+(cryptand[2.2.2J) electride and evidence for trapped electron pairs, Nature. 1988;331: 599–601.

[44] F.J. Tehan, B.L. Barnett, J.L. Dye, et al. Alkali anions. Preparation and crystal structure of a compound which contains the cryptated sodium cation and the sodium anion, J. Am. Chem, Soc. 1974; 96: 7203–7208.

[45] J.L. Dye, Electrides: Early Examples of Quantum Confinement, Acc. Chem. Res. 42 2009; 1564–1572.

[46] J. Cao, F. Li, W. Xia, et al. van der Waals interactions in bimolecular reactions, Chin. J. Chem. Phys. 2019; 32: 157–166.

[47] Z. Shen, H. Ma, C. Zhang, et al. Dynamical Importance of van der Waals Saddle and Excited Potential Surface in C(^{1}D)+D2 Complex-forming Reaction, Nat. Commun. 2017; 8: 14094.

[48] M.J. Frisch, G.W. Trucks, H.B. Schlegel, et al. Gaussian 09, 2009.

[49] F. Neese, F. Wennmohs, U. Becker,et al. The ORCA quantum chemistry program package, J. Chem. Phys. 2020; 152: 224108.

[50] J.-D. Chai, M. Head-Gordon, Long-range corrected hybrid density functionals with damped atom–atom dispersion corrections, Phys. Chem. Chem. Phys. 2008; 10: 6615–6620.

[51] P. Pérez, A. Toro-Labbé, R. Contreras, Solvent effects on electrophilicity, J. Am. Chem. Soc. 2001; 123: 5527–5531.

[52] H. Chermette, Chemical reactivity indexes in density functional theory, J. Comput. Chem. 1999; 20: 129–154.

[53] F. Castet, V. Rodriguez, J.L. Pozzo, et al. Design and Characterization of Molecular Nonlinear Optical Switches, Acc. Chem. Res. 2013; 46: 2656.

[54] I. Asselberghs, C. Flors, L. Ferrighi,et al. Van der Auweraer, K. Clays, Second-Harmonic Generation in GFP-like Proteins, J. Am. Chem. Soc. 2008; 130: 15713–15719.

[55] I. Cukrowski, J.H. de Lange, A.S. Adeyinka, et al. Evaluating common QTAIM and NCI interpretations of the electron density concentration through IQA interaction energies and 1D cross-sections of the electron and deformation density distributions, Comput. Theor. Chem. 2015; 1053: 60–76.

[56] A. Allouche, Software News and Updates Gabedit-A Graphical User Interface for Computational Chemistry Softwares, J. Comput. Chem. 2012; 32: 174–182.

[57] F. Fuster, A. Sevin, B. Silvi, Topological Analysis of the Electron Localization Function (ELF) Applied to the Electrophilic Aromatic Substitution, J. Phys. Chem. A. 2000; 104:852–858.

[58] R.J. Clements, J.C. Womack, C.K. Skylaris, Electron localisation descriptors in ONETEP: A tool for interpreting localisation and bonding in large-scale DFT calculations, Electron. Struct. 2020; 2.

[59] N. V Tkachenko, Z.-M. Sun, A.I. Boldyrev, Record Low Ionization Potentials of Alkali Metal Complexes with Crown Ethers and Cryptands, ChemPhysChem. 2019; 20: 2060–2062.

[60] A.N. Chekhlov, Synthesis and crystal structure of (2.2.2-cryptand)potassium nitrate hydrate, Russ. J. Coord. Chem. 2006; 32: 5–9.

[61] N. Kosar, L. Zari, K. Ayub, et al. NLO properties and electride characteristics of superalkalis doped all-cis-1,2,3,4,5,6-hexafluorocyclohexane complexes, Optik. 2022; 271: 170139.

[62] D. V Konarev, S.S. Khasanov, M. Ishikawa, et al. Metallic conductivity versus charge disproportionation in C_{60} complexes with noninteger average charges on fullerene, ChemistrySelect. 2016; 1:323–330.

[63] E. Rehm, A.I. Boldyrev, P. v R. Schleyer, Ab initio study of superalkalis. First ionization potentials and thermodynamic stability, Inorg. Chem. 1992; 31: 4834–4842.

[64] A. Ahsin, T. Jadoon, K. Ayub, M@[12-crown-4] and M@[15-crown-5] where (M=Li, Na, and K); the very first examples of non-conventional one alkali metal-containing alkalides with remarkable static and dynamic NLO response, Phys. E Low-Dimensional Syst. Nanostructures. 2022; 140: 115170.

[65] A. Ahsin, A.B. Shah, K. Ayub, Germanium-based superatom clusters as excess electron compounds with significant static and dynamic NLO response; a DFT study, RSC Adv. 2022; 12: 365–377.

[66] J.-J. Wang, Z.-J. Zhou, Y. Bai, et al. A new strategy for simultaneously enhancing nonlinear optical response and electron stability in novel cup–saucer+-cage−-shaped sandwich electride molecules with an excess electron protected inside the cage, Dalt. Trans. 2015; 44: 4207–4214.

[67] A. Ahsin, I. Ejaz, S. Sarfaraz, K. Ayub, H. Ma, Polaron Formation in Conducting Polymers: A Novel Approach to Designing Materials with a Larger NLO Response, ACS Omega. 2024;9:14043-14053.

[68] F. Ullah, N. Kosar, K. Ayub, et al. Superalkalis as a source of diffuse excess electrons in newly designed inorganic electrides with remarkable nonlinear response and deep ultraviolet transparency: A DFT study, Appl. Surf. Sci. 2019; 483:1118–1128.

[69] N. Kosar, L. Zari, K. Ayub, et al. Giant NLO response and ultraviolet transparency of superalakalis decorated $C_6O_6Li_6$ complexes; a DFT perspective, Phys. Scr. 2023, 98 65909.

[70] Y.-F. Wang, J. Huang, L. Jia, et al, Theoretical investigation of the structures, stabilities, and NLO responses of calcium-doped pyridazine: alkaline-earth-based alkaline salt electrides, J. Mol. Graph. Model. 2014; 47: 77–82.

[71] M.D. Williams, J.S. Ford, D.L. Andrews, Hyper-Rayleigh scattering in centrosymmetric systems, J. Chem. Phys. 2015; 143: 124301.

[72] M.R. Maina, Y. Okamoto, K. Hamada, et al. Effects of superposition of 532 nm and

1064 nm wavelengths in copper micro-welding by pulsed Nd:YAG laser, J. Mater. Process. Technol. 2022; 299-311:

[73] S. Abel, F. Eltes, J.E. Ortmann, et al. Large Pockels effect in micro- and nanostructured barium titanate integrated on silicon, Nat. Mater. 2019; 18: 42–47.

[74] Q. Shi, L. Dong, Y. Wang, Evaluating refractive index and birefringence of nonlinear optical crystals: Classical methods and new developments, Chines J. Struct. Chem. 2023; 42: 100017.

[75] Q. Lu, W. Bian, The Decay of Dispersion Interaction and Its Remarkable Effects on the Kinetics of Activation Reactions Involving Alkyl Chains, J. Phys. Chem. Lett. 2023; 14: 10642–10647.

[76] X. Yang, H. Ma, Q. Lu, et al. Efficient Method for Numerical Calculations of Molecular Vibrational Frequencies by Exploiting Sparseness of Hessian Matrix, J. Phys. Chem. A. 2023;128:2909-3046.

[77] F. Li, X. Yang, X. Liu, et al. An Ab *Initio* Neural Network Potential Energy Surface for the Dimer of Formic Acid and Further Quantum Tunneling Dynamics, ACS Omega. 2023; 8: 17296-17303.

[78] F. Li, X. Liu, X. Yang, et al. Quantum Dynamics Calculations on Isotope Effects of Hydrogen Transfer Isomerization in Formic Acid Dimer, Chin. J. Chem. Phys. 2023; 36: 545-552.

[79] Y. Wu, J. Cao, H. Ma, at al. Conical intersection–regulated intermediates in bimolecular reactions: Insights from C(^{1}D) + HD dynamics, Sci. Adv. 2019;5: 2375-2548

[80] J. Cao, Y. Wu, W. Bian, Ring polymer molecular dynamics of the C(^{1}D)+H_2 reaction on the most recent potential energy surfaces, Chin. J. Chem. Phys. 2021; 34:833–842.

[81] C. Zhang, M. Fu, Z. Shen, et al. Global analytical ab initio ground-state potential energy surface for the C(^{1}D)+H_2 reactive system, J. Chem. Phys. 2014; 140: 234301-234310

[82] M. Michalski, A.J. Gordon, S. Berski, Topological analysis of the electron localisation function (ELF) applied to the electronic structure of oxaziridine: the nature of N-O bond, Struct. Chem. 2019; 30: 2181–2189.

Figure 1: Representation of optimized labeled geometries (a) pure diazacryptand [2.2.2] and (b) M@crypt complexes using the ωB97xd/def2-tzvp level of theory.

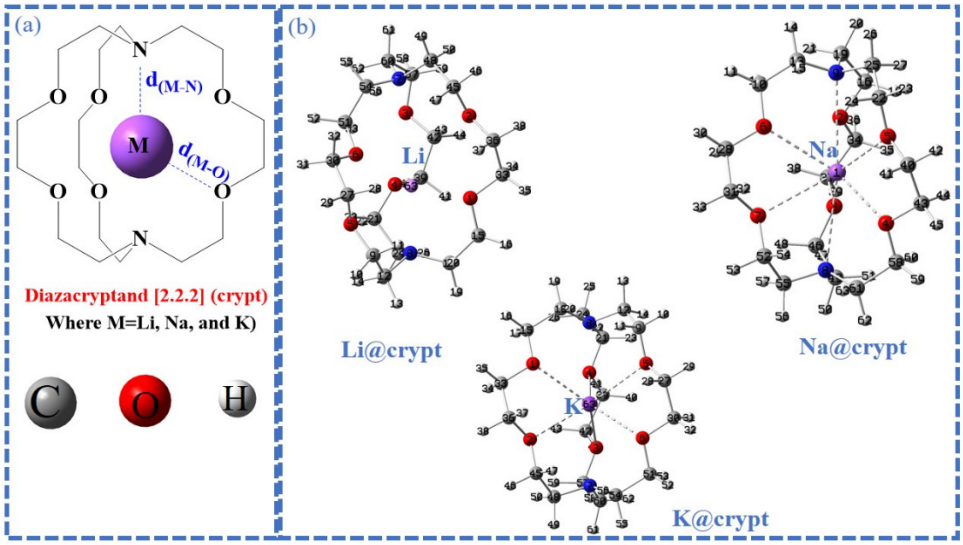

Figure 2: 3D representation of frontier molecular orbitals (FMOs) involved in electronic excitations of designed complexes using the ωB97xd/def2-tzvp method. (isovalue =0.015)

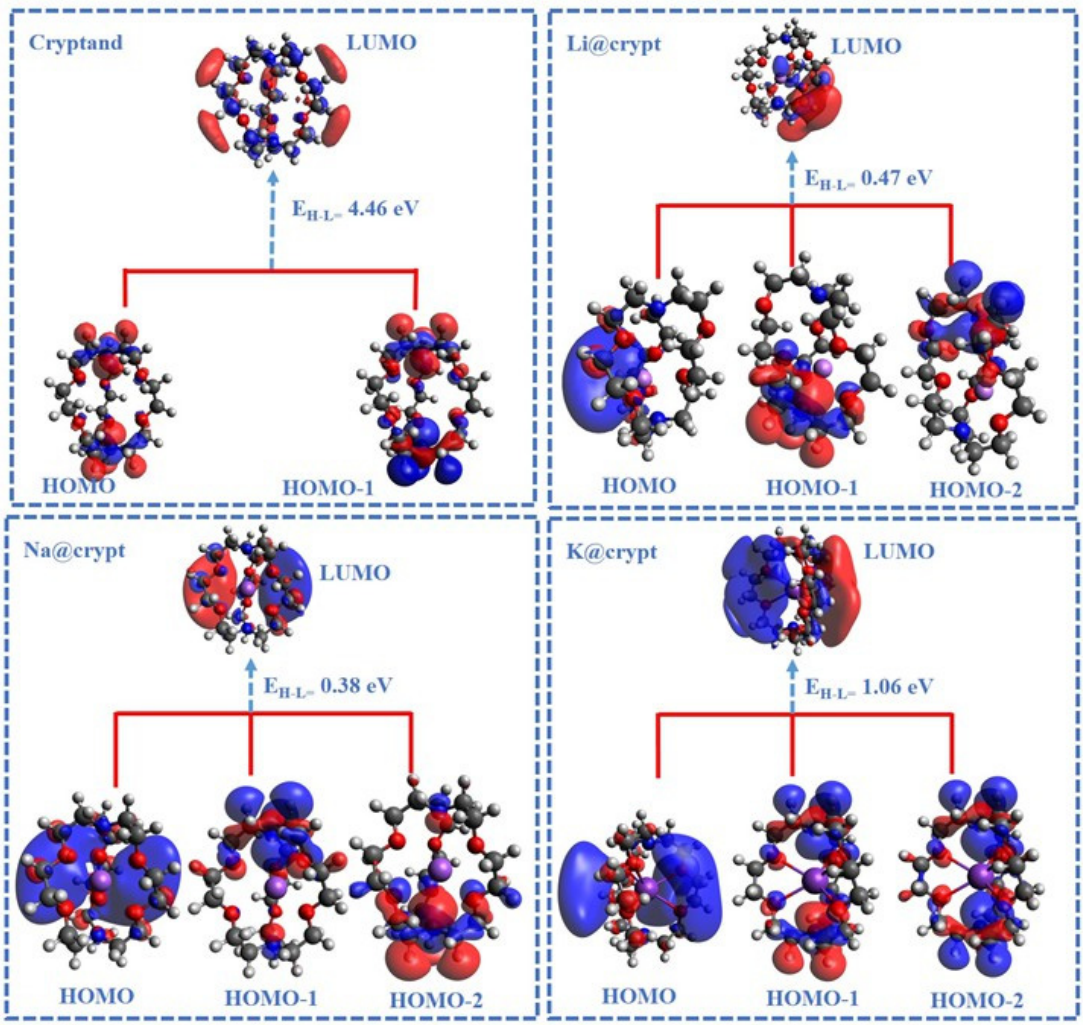

Figure 3: (a) Representation of labeled geometries for generated bond critical points (BCP) by considering the (3, -1) electron density, (b) (RDG) map of complexes using the ωB97xd/def2-tzvp level of theory.

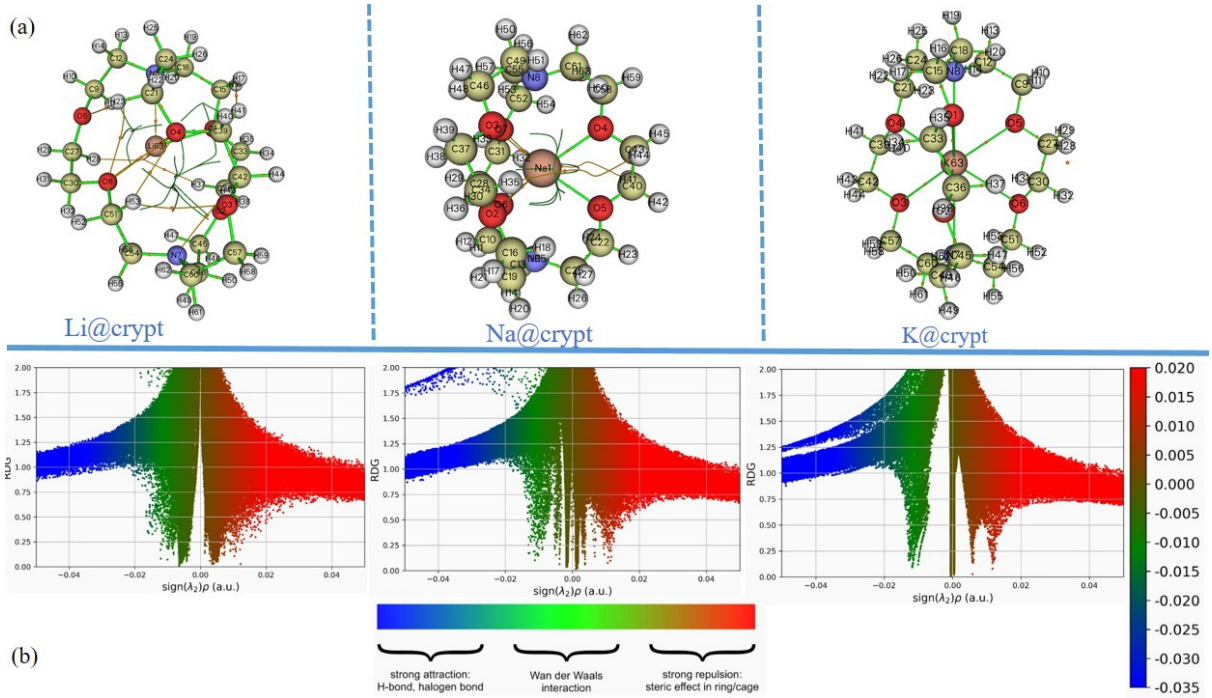

Figure 4: Topological spectra (a) electron localizing function, (b) localized orbital locator (LOL) of crypt and M@crypt electrides using the ωB97xd/def2-tzvp method.

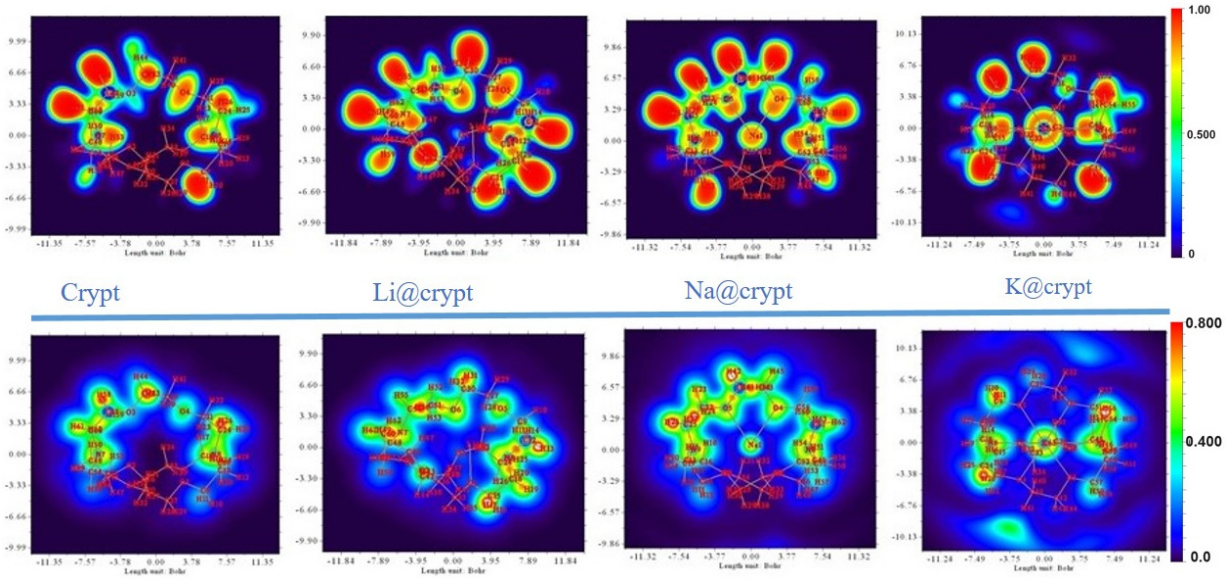

Figure 5: Absorbance spectra of present complexes using the TD- ωB97xd/def2-tzvp method.

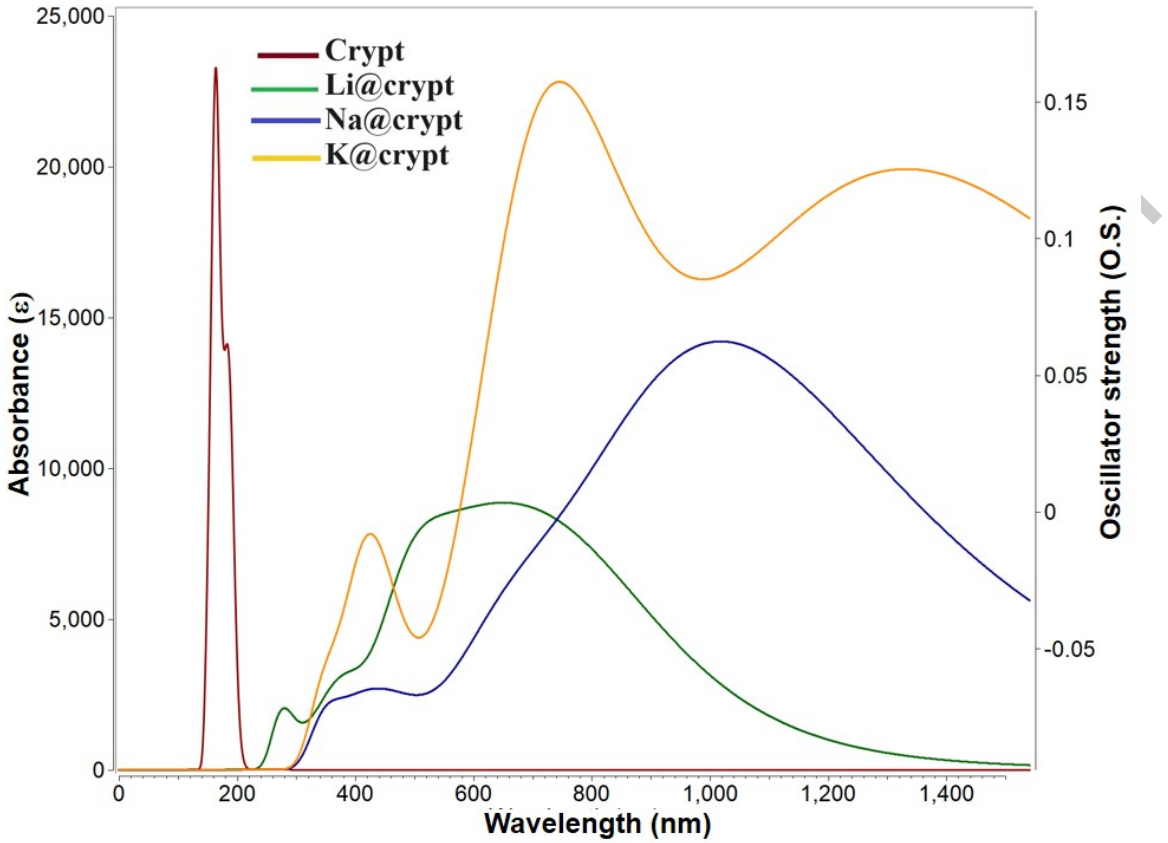

Table 1: Interaction energies (E_{int} kcal/mol), vertical ionization potential (VIP eV), vertical electron affinity (VEA eV), chemical hardness (ɳ eV), , HOMO and LUMO energies (in eV), energy gap (E_{H-L} eV), NBO charge on alkali metals (QM |e|), NBO charge in nitrogen (QN |e|), and highest NBO charge on oxygen (QO |e|) of complexes.

	E_{int}	VIP	VEA	ɳ	E_{HOMO}	E_{LUMO}	E_{H-L}	Q(M)	Q(N)	Q(O)
Crypt	N/A	7.56	3.14	4.42	-7.60	-3.18	4.46	N/A	-0.42	-0.49
Li@Crypt	-21.91	1.90 2.05[a]	2.01	0.47	-2.12	2.59	0.47	0.04	-0.65	-0.63
Na@Crypt	-11.10	1.01 1.96[a]	1.43	0.38	-1.17	1.55	0.38	0.01	-0.60	-0.64
K@Crypt	-20.56	1.08 1.95[a]	0.80	1.07	-1.14	2.21	1.06	-0.0001	-0.58	-0.65

[a] Values were reported using the PBE0/6-311++G** method [61].

Table 2: Mean dipole moment (μ_o Debye), polarizability and its components (α_o au), hyperpolarizability and its components (β_o au), and projection of hyperpolarizability on dipole moment vector (β_{vec} au).

	μ_o	α_o	α_x	α_y	α_z	β_o	β_x	β_y	β_z	β_{vec}
Crypt	0	2.54×10^{2}	2.76×10^{2}	2.42×10^{2}	2.42×10^{2}	1.02×10^{2}	25.00	96.16	24.67	6.489
Li@crypt	4.69	3.47×10^{2}	4.14×10^{2}	3.38×10^{2}	2.89×10^{2}	5.32×10^{3}	3.48×10^{3}	6.45×10^{2}	3.97×10^{3}	3.59×10^{3}
Na@crypt	6.04	8.66×10^{2}	6.56×10^{2}	5.01×10^{2}	3.75×10^{3}	1.41×10^{6}	2.57×10^{4}	1.19×10^{6}	7.64×10^{5}	1.19×10^{6}
K@crypt	0.10	9.30×10^{2}	6.12×10^{2}	1.10×10^{3}	1.07×10^{2}	9.83×10^{5}	2.41×10^{5}	9.50×10^{5}	5.56×10^{4}	2.96×10^{5}

Table 3: Static second hyperpolarizability (β_o au) scattering hyperpolarizability (β_{HRS} au), depolarization ratio (DR), percentage dipolar contribution to hyperpolarizability Φβ(j=1), and octupolar contribution to hyperpolarizability Φβ(j=3) of Crypt and M@crypt complexes.

Complexes	γ_o	γ_x	γ_y	γ_z	β_{HRS}	DR	Φβ(j=1)	Φβ(j=3)
Crypt	1.05×10^{4}	6.9810^{3}	5.5610^{3}	5.5710^{30}	170.21	1.500	0.1	99.9%
Li@crypt	4.30×10^{5}	4.03×10^{5}	1.45×10^{5}	3.97×10^{4}	1.33×10^{4}	4.60	52%	48%
Na@crypt	2.96×10^{8}	3.88×10^{7}	2.92×10^{8}	3.53×10^{7}	9.01×10^{5}	2.51	34%	66%
K@crypt	4.96×10^{9}	1.04×10^{8}	2.23×10^{7}	4.94×10^{9}	1.31×10^{6}	3.53	44%	56%

Table 4: Frequency-dependent NLO properties; EOPE β(-ω, ω,0), ESHG β(-2ω,ω,ω), dc-Kerr effect γ(-ω, ω,0,0), and SHG γ(-2ω,ω,ω,ω) at 532 and 1064 nm.

	Frequency-dependent hyperpolarizability β(ω) using ωB97xd/def2-tzvp			
	532.37nm (ω=0.085645 au)		1064.73nm (ω=0.042823 au)	
	β(-ω, ω,0)	β(-2ω, ω, ω)	β(-ω,ω,0)	β(-2ω,ω,ω)
Crypt	0.60	0.64	0.590	0.60
Li@crypt	7.99×10^{3}	4.99×10^{4}	7.99×10^{4}	2.98×10^{4}
Na@crypt	1.34×10^{4}	5.80×10^{4}	9.55×10^{7}	6.62×10^{4}
K@crypt	1.11×10^{5}	7.90×10^{4}	7.50×10^{3}	7.90×10^{4}
	Frequency-dependent second hyperpolarizability γ(ω) using ωB97xd/def2-tzvp			
	γ(-ω, ω,0,0)	γ (-2ω,ω,ω,ω)	γ(-ω,ω,0,0)	γ (-2ω,ω,ω,0)
Crypt	1.20×10^{4}	1.6×10^{4}	1.0×10^{4}	1.16×10^{4}
Li@crypt	1.53×10^{8}	1.85×10^{7}	1.18×10^{6}	6.26×10^{6}
Na@crypt	2.48×10^{8}	1.47×10^{7}	7.36×10^{12}	2.59×10^{12}
K@crypt	2.83×10^{7}	3.09×10^{7}	2.70×10^{7}	6.38×10

Table 5: Excitation energy (ΔE in eV), absorbance wavelength (λ_{max} in nm), oscillator strength (O.S. au), and percentage contribution of orbitals during crucial transitions

TD-DFT Parameters from Crucial Transitions				
Complexes	ΔE	wavelength (λ_{max})	O.S.	Percentage contributions of orbitals
Crypt	7.73	160	0.14	
Li@Crypt	1.58	783	0.13	HOMO→LUMO (43.8%) HOMO→LUMO+1 (32%) HOMO→LUMO+4 (4.8%)
Na@Crypt	1.22	1016	0.24	HOMO→LUMO+3 (86%) HOMO→LUMO+5 (10%) HOMO→LUMO+2 (1.5%)
K@Crypt	1.66	746	0.24	HOMO→LUMO (79%) HOMO→LUMO+1 (18.2%) HOMO→LUMO+5 (1.3%)

Statement of Novelty /Impact statement

Organic electrides M@cryptand [2.2.2] (where M=Li, Na, and K) were examined. Excess electrons and vdW forces play critical roles in promoting the NLO responses.

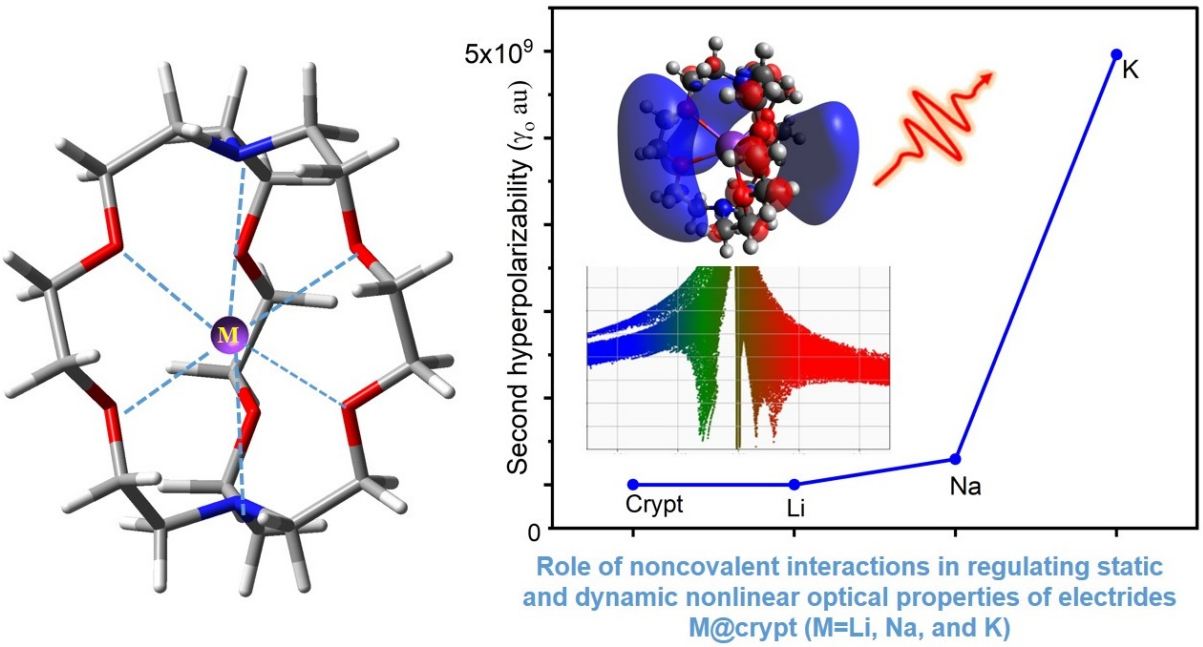

Role of noncovalent interactions in regulating static and dynamic nonlinear optical properties of electrides M@crypt (M=Li, Na, and K)

GA

Supplementary information for:

Theoretically designed M@diaza[2.2.2]cryptand complexes: the role of non-covalent interactions in promoting NLO properties of organic electrides

Atazaz Ahsin[1,3] Aamna Qamar[2,3] Qing Lu[1*] Wensheng Bian[1,3*]

[1]Beijing National Laboratory for Molecular Sciences, Institute of Chemistry, Chinese Academy of Sciences, Beijing 100190, China,

[2]Beijing National Laboratory for Molecular Sciences, State Key Laboratory of Polymer Physics and Chemistry, Chinese Academy of Sciences, Beijing 100190, China

[3]School of Chemical Sciences, University of Chinese Academy of Sciences, Beijing 100049, China

Correspondence[*]:)，qinglu@iccas.ac.cn (Q. L), bian@iccas.ac.cn (W. B)

Table of Contents

Table S1: Optimized geometrical parameters, bond distances are (in Å)

Calculated at the ωB97xd/def2-tzvp		Experimental	
Diaza(2.2.2)cryptand (crypt)			
Bond type	magnitude		
C-C in CH_2-CH_2	1.50	C-C	1.48
C-H	1.10	C-H	1.09
C-O1/O2/O3/O4/O5/O6	1.40	C-O	1.41
N8-C12/18/24 N7-C54/C48/C60	1.44	N-C	1.46
Li@crypt			
C-C	1.51	C-C	
C-H	1.09	C-H	
C-O	1.40	C-O	
N-C	1.45	N-C	
Li63-N7	3.95		
Li63-N8	2.46		
Li63-O3/O4/O3/O6	4.5/2.34/2.70/2.70		
Na@crypt			
Na1-N8/N9	3.19		
Na1-O4/O5	2.488		
Na1-O2/O3	2.89/2.82		
Na1-O7/O6	2.89/2.82		
K@crypt		[K(Crypt-222)](NO3) 1.5H2O [1]	
C-C	1.51	C-C	1.49
C-H	1.09	C-H	1.08
C-O	1.40	C-O	1.41
N-C	1.45	N-C	1.46
K63-N7/N8	3.07	K63-N7/N8	2.94/2.97
K63-O1/O2	2.83	K63-O3/O4	2.83/2.78
K63-O3/O4 K-O	2.82/2.83 2.83 [50][b]	K63-O3/O4	2.77/2.87

[b] Average reported distance between oxygen atoms and K-metal in K[2.2.2]

Table S2: The calculated and experimentally reported vibrational frequencies of pure (cryptand) and designed complexes using the ωB97xd/def2-tzvp. The calculated stretching vibration are corrected by multiplying 0.96 in order to get comparison with experimental values

	Frequency (cm^{-1})			
	Calculated at the ωB7XD/def2-tzvp	Experimental [3]	Group	Vibration
Cryptand	2812	2790-2877	C-H	Stretching
	2896		C-H	Stretching
	2981		C-H	Stretching
	1523	1452	C-H	Bending
	1173-1181	1295	C-N	Stretching
	1158.72	1111-1127	C-O	Stretching
	1047-1063	1038-1078	C-C	Stretching
Li@crypt				
	2782-3004		C-H	Stretching
	1274- 1533		C-H	Bending
	1168-1181		C-N	Stretching
	1109-1156		C-O	Stretching
	1067		C-C	Stretching
Na@crypt				
	2826-2990		C-H	Stretching
	1224-1495		C-H	Bending
	1157-1176		C-N	Stretching
	1090-1157		C-O	stretching
	1059-1075		C-C	Stretching
K@crypt	2833- 2998		C-H	Stretching
	1275-1526		C-H	Bending
	1168-1172		N-C	Stretching
	1173-1157		C-O	Stretching
	1059-1066		C-C	Stretching

Discussion on electride nature and comparison with reported similar system

The energy of the highest occupied molecular orbitals (E_{HOMO}), lowest unoccupied molecular orbitals (E_{LUMO}), and HOMO-LUMO gaps ($E_{H\text{-}L}$) have significant roles in determining the reactivity of molecules. The HOMO energies of designed complexes are -2.12, -1.17, and -1.46 eV, while LUMO energies lie in the range of -2.59, 1.55, and 2.21 eV for **Li@crypt**, **Na@crypt**, and **K@crypt** (Table 1). The HOMO energies are increasing from Li to K with increased atomic number, while a significant reduction in HOMO-LUMO gaps is observed for complexes as compared to pure complexant. The $E_{H\text{-}L}$ gaps are from 0.47, 0.38, and 1.06 eV, respectively, for **Li@crypt**, **Na@crypt**, and **K@crypt,** where the lowest value is obtained for **Na@crypt** complex. Overall, the values are significantly reduced as compared to $E_{H\text{-}L}$ of the pristine crypt (4.46 eV). The contribution of HOMO-1 and the energy difference HOMO-1 to LUMO are also given in Figure 2. The obtained HOMO-LUMO gaps of present complexes are significantly lower than those of superalkali@$F_6C_6H_6$ and M(BCM) complexes at the ωB97xd/def2tzvp method [4][5].

Table S3: The comparison of electronic properties with reported similar complexes having electrides nature and simply excess electrons compounds.

Alkali and alkaline doped benzocryptand M(BC)M at B3LYP/6-31(G) [4]				
	E_{int} (kcal/mol)	**E_{H-L} (eV)**	**VIP (eV)**	**Ƞ (eV)**
Li(BC)Be	−9.72	1.21	1.97	0.61
Na(BC)Be	−9.73	1.14	1.96	0.57
K(BC)Be	−0.43	2.23	2.95	1.12
Superalkali@ $C_6S_6Li_6$ at the ωb97xd/6–31+*G*(d,p) [6]				
$Li_3O@C_6S_6Li_6$	−45.56	1.69	2.20	
$Na_3O@C_6S_6Li_6$	−42.86	1.68	2.18	
$K_3O@C_6S_6Li_6$	−43.35	2.33	2.63	
Superalkalis doped $F_6C_6H_6$ at the ωb97xd/6–31+G (d,p) [5]				
$Li_2F@C_6F_6H_6$	-16.54	2.50	3.02	
$Li_2Cl@C_6F_6H_6$	-14.57	3.78	3.87	
$Li_2Br@C_6F_6H_6$	-16.52	3.41	3.75	
$Na_2F@C_6F_6H_6$	-13.57	2.42	2.91	
$Na_2Br@C_6F_6H_6$	-13.98	3.58	3.81	
$K_2F@C_6F_6H_6$	-14.28	1.97	2.49	
$K_2Cl@C_6F_6H_6$	-14.51	3.48	3.48	

Table S4: Polarizability (α_o au), hyperpolarizability (β_o au), and projection of hyperpolarizability on dipole moment vector (β_{vec} au).

	ωB97xd/def2-tzvp			CAM-B3LYP/def2-tzvp			M062X/def2-tzvp		
	α_o	β_o	β_{vec}	α_o	β_o	β_{vec}	α_o	β_o	β_{vec}
Crypt	2.54×10^{2}	1.02×10^{2}	6.489	2.53×10^{2}	0.037	0.009	2.5×10^{2}	16.729	15.287
Li@crypt	3.47×10^{2}	5.32×10^{3}	3.59×10^{3}	3.56×10^{2}	3.96×10^{3}	9.62×10^{2}	3.5×10^{2}	3.9×10^{3}	9.6×10^{2}
Na@crypt	8.66×10^{2}	1.41×10^{6}	1.19×10^{6}	1.41×10^{3}	4.18×10^{5}	4.18×10^{5}	5.3×10^{2}	3.2×10^{4}	3.2×10^{4}
K@crypt	9.30×10^{2}	9.83×10^{5}	2.96×10^{5}	7.75×10^{3}	2.93×10^{3}	2.93×10^{2}	1.1×10^{3}	2.5×10^{6}	3.1×10^{5}

Table S5: Comparison of static first and second hyperpolarizability (in au) of designed complexes with reported electrides and excess electrons compounds.

Our studied Complexes M@Crypt (where M=Li, Na, and K)		
Complexes	**β_o (ωb7xd/def2-tzvp)**	**γ_o**
Crypt	1.02×10^{2}	-
Li@crypt	5.32×10^{3}	1.72×10^{10}
Na@crypt	1.41×10^{6}	2.57×10^{11}
K@crypt	9.83×10^{5}	2.87×10^{4}
$C_6S_6Li_6$@Superalkali at ωb97xd/6–31+*G*(d,p) level [6]		
$C_6S_6Li_6$	2.65	
$Li_3O@C_6S_6Li_6$	4.54×10^{6}	2.06×10^{10}
$Na_3O@C_6S_6Li_6$	2.09×10^{6}	9.62×10^{12}
$K_3O@C_6S_6Li_6$	2.98×10^{5}	2.25×10^{8}
Superalkali@$C_6F_6H_6$ at ωb97xd/6–31+G (d,p) level of theory [5]		
$Li_2F@C_6F_6H_6$	9.32×10^{4}	3.44×10^{7}
$Li_2Cl@C_6F_6H_6$	3.26×10^{4}	5.69×10^{6}
$Li_2Br@C_6F_6H_6$	8.49×10^{3}	5.07×10^{8}
$Na_2F@C_6F_6H_6$	1.68×10^{6}	3.35×10^{7}
$Na_2Br@C_6F_6H_6$	1.77×10^{4}	3.18×10^{4}
$K_2F@C_6F_6H_6$	4.07×10^{5}	1.52×10^{8}
$K_2Cl@C_6F_6H_6$	3.89×10^{4}	1.39×10^{7}
$Li_3@C_{60}$ and $Li_3@B_{40}$ electrides [7]		
$Li_3@C_{60}$	129.4	3.6×10^{5}
$Li_3@B_{40}$	79.9	2.1×10^{5}

Alkali and Alkaline metals doped M(BC)M benzocryptand [4]		
Li(BC)Be	$2.0\,89\times 10^{4}$	
Na(BC)Be	2.35×10^{4}	
K(BC)Be	3.39×10^{3}	

Table S6: QTAIM and its parameters at BCP (3,-1) of M@crypt complexes: value are in a.u

Li@crypt						
CP	Interactions	ρ_r	∇^2_ρ	G_r	V_r	H_r
120	N8—Li63	0.0098	0.0578	0.1131	-0.0081	0.0031
109	O1-- Li63	0.0123	0.9642	0.0185	-0.0561	0.0067
116	04-- Li63	0.9011	0.0634	0.0119	-0.0080	0.0039
141	O6-- Li63	0.0117	0.0845	0.0160	-0.0116	0.0050
127	O4—H53	0.869	0.0337	0.0079	-0.0052	0.0015
93	O1--04	0.0066	0.02543874	0.0050	-0.0037	0.0013
131	O4--06	0.0087	0.0972156	0.0079	-0.0067	0.0019
146	N7—C54	0.2748	-0.7203550	0.1186	-0.4174	-0.2987
107	O4—C21	0.2620	-0.5610097	0.2283	-0.5977	-0.3686
Na@crypt						
99	O7-Na1	0.4782	0.2578	0.0048	-0.0032	0.1612
123	O4-NA1	0.0130	0.0048	0.0160	-0.0112	0.0048
93	O6-Na1	0.5327	0.0303	0.0056	-0.3702	0.0019
105	O2-Na1	0.4779	0.0257	0.0048	-0.0032	0.0016
120	O5-Na1	0.0138	0.0834	0.0160	-0.0111	0.0048
K@crypt						
104	O1--K63	0.0127	0.0640	0.0127	-0.0094	0.3296
106	O2--K63	0.0127	0.0640	0.0127	-0.0094	0.0032
100	O3--K63	0.0128	0.0487	0.0128	0.0095	0.0033
95	O4--K63	0.0128	0.0646	0.0128	-0.0095	0.0033
128	O5--K63	0.0128	0.0648	0.0128	-0.0095	0.0033
130	O6--K63	0.0128	0.0647	0.0128	-0.0095	0.3003
111	N8-K63	0.0100	0.0403	0.0088	-0.0061	0.0019
118	N8-K63	0.0100	0.0403	0.0081	-0.0061	0.0019
145	O6-H37	0.0047	-0.0019	0.0007	-0.00003	-0.0004
98	O2—C36	0.2650	-0.5758	0.2316	-0.6073	-0.3756

Discussion of EDDM and DOS study of complexes

An electronic density difference map (EDDM) is used to predict the charge transferability and distribution of orbital after the relaxation of the electron from an excited state to a ground state ($\rho_{excited} - \rho_{ground}$). From EDDM pictures, distinct colors (purple, cyan-blue) depict various orbital densities in different regions of complexant. The 3D-mapped EDDM spectra are given in Figure S4. Purple is used to represent the nucleophilic zone, where electron density drops with charge transfer, and cyan-blue is used to represent the electrophilic region, where electron density increases with charge transfer. For **Li@crypt,** orbital density is higher in the lower region of the complex, which might be due to strong interaction with N7 and significant charge transfer. Likewise, the complex **Na@crypt** shows a distribution of electron density close to Na-metals in the middle of the cavity. In **K@Crypt**, the K-metal adsorbed in the center of the complexant, and the charge transfer effect is uniform throughout the cryptand.

The plotted TDOS of pure (crypt) is shown in Figure S6, while the projected density of state (PDOS) is shown in Figure S5. For the pristine crypt, the TDOS spectra are plotted between an energy range of -20 to 20 eV, and the HOMO line appears near -7 eV. The HOMO-LUMO gap is also wider for pristine crypt. Likewise, in PDOS spectra, the contribution of alkali metals as fragments displayed a crucial role in narrowing the HOMO-LUMO gaps. The red color indicates the contribution from the main complexant, while the blue color line shows the contribution to the density of states from alkali metals.

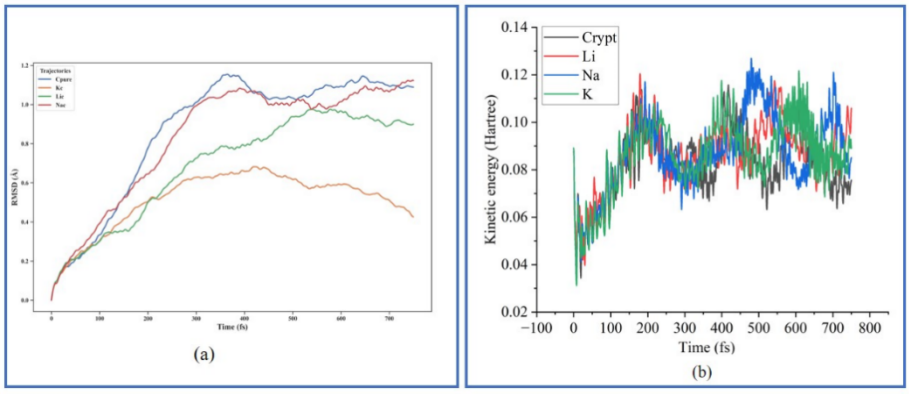

Figure S1: AIMD analysis of complexes. **(a) root-mean-square deviation (RMSD), (b) Kinetic energy of crypt and M@crypt complexes at 300 K and 750 (time fs) using the B3LYP-D3/def2-SVP method.**

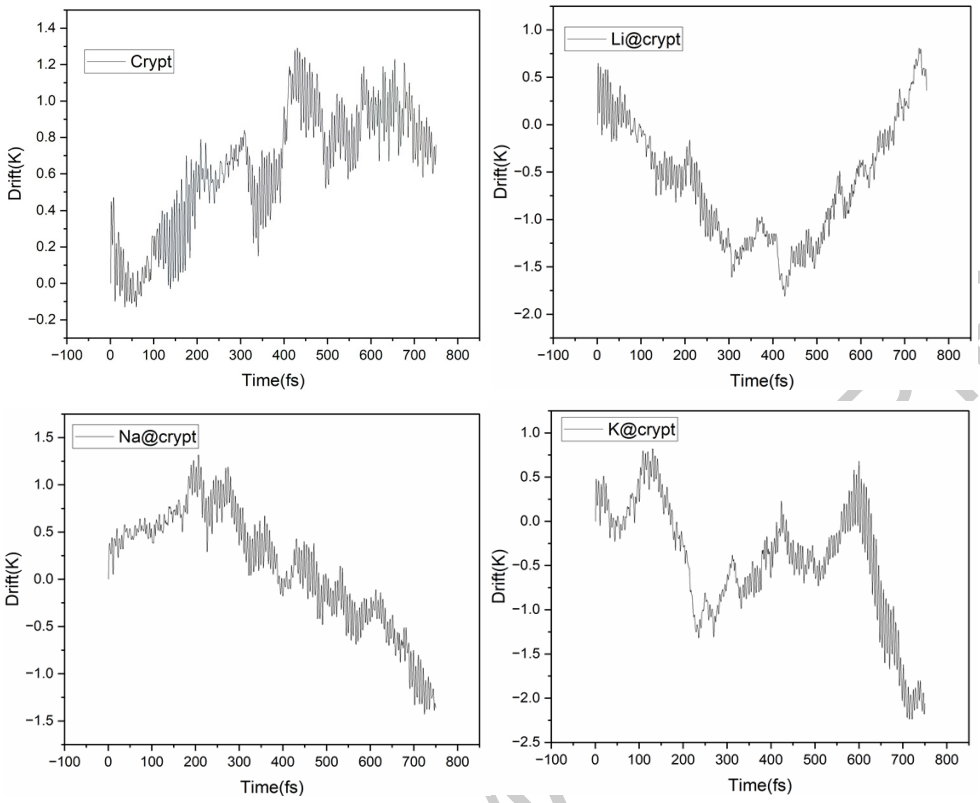

Figure S2: Drift energy (K) versus time of pure and M@crypt complexes at 300 K during the ab-initio molecule dynamic (AIMD) simulation using the B3LYP-D3/def2-SVP method.

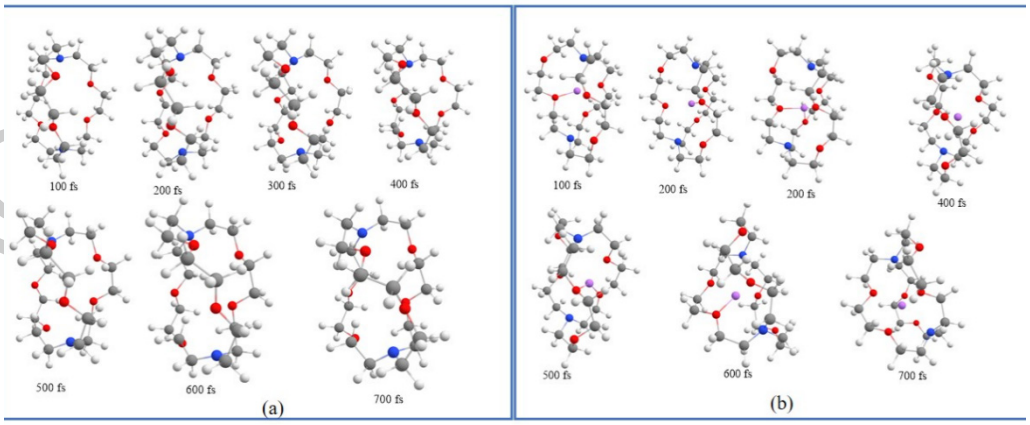

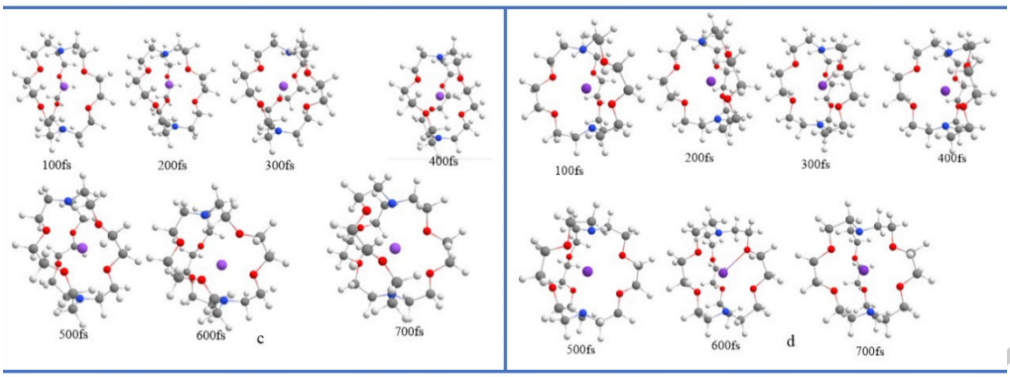

Figure S3: Snapshots of pure and designed complexes during 750 fs using 1500 steps**.** (a) shows the pure (diaza cryptand[2.2.2]), (b) Li@crypt, (c) Na@crypt, (d) K@crypt during AIMD study.

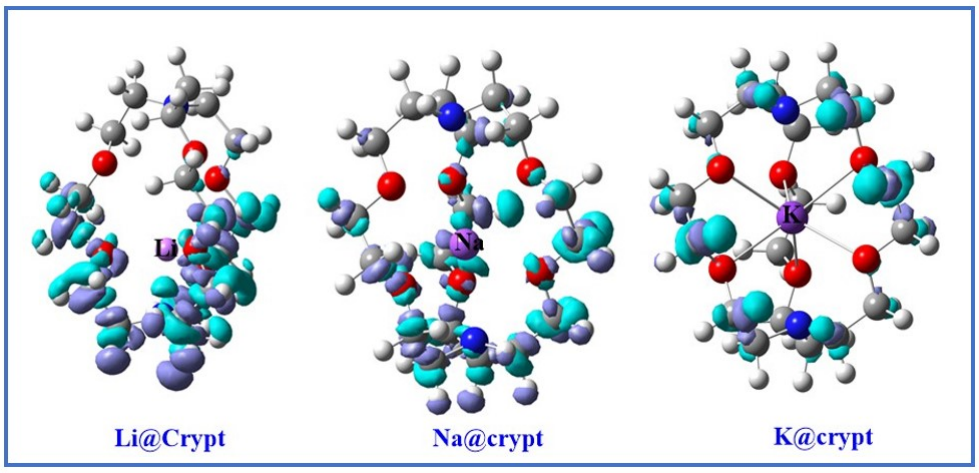

Figure S4: Molecular orbitals from EDDM analysis of designed electrides complexes

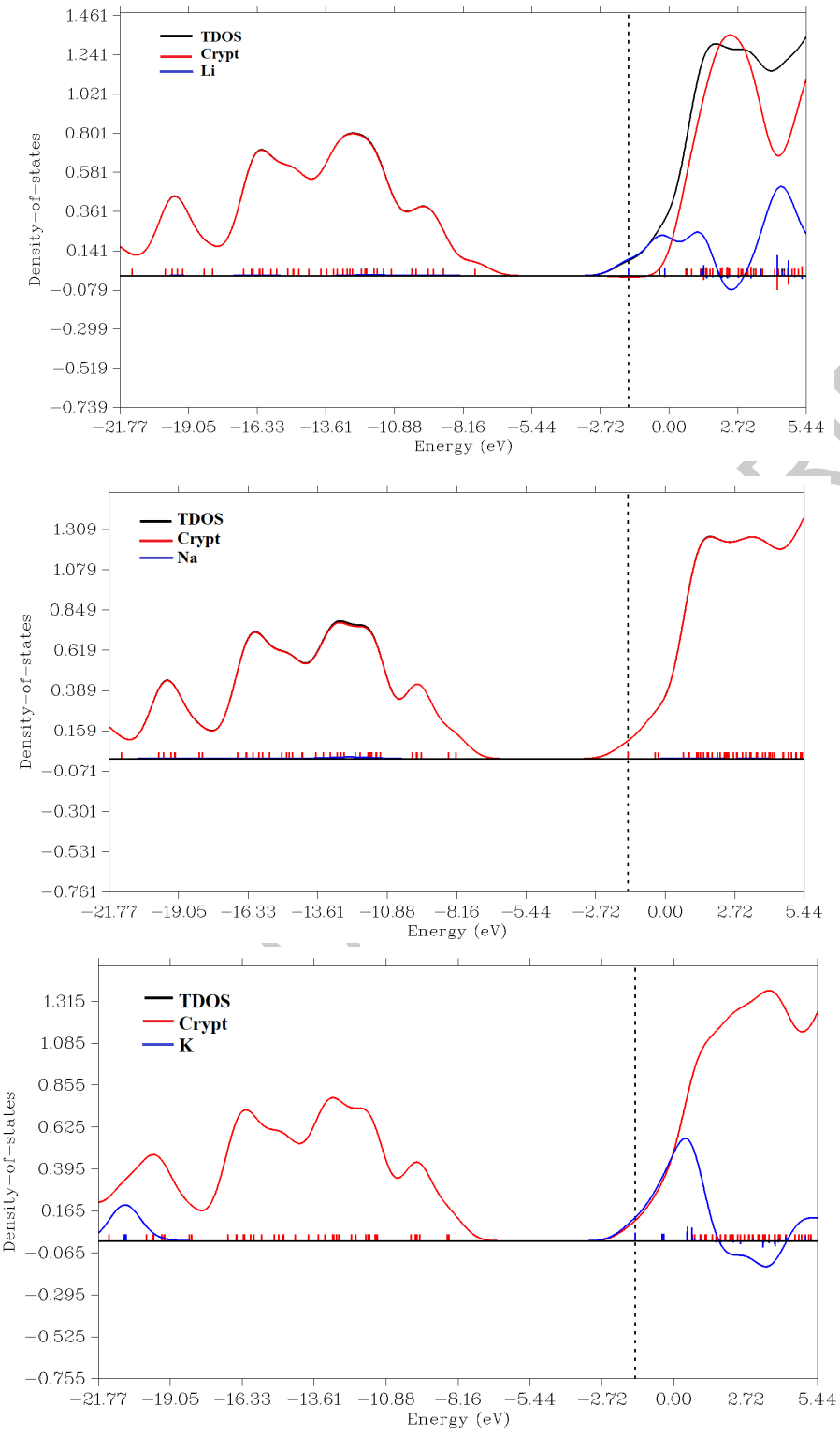

Figure S5: projected density of states (PDOS) spectra of electrides: blue curve show the contribution of metals to orbitals while red line for complexant. The black curve is representing total density of states using the ωB97xd/def2-tzvp method

References

[1] A.N. Chekhlov, Synthesis and crystal structure of (2.2.2-cryptand)potassium nitrate hydrate, Russ. J.

Coord. Chem. Khimiya. 2006; 32: 5–9.

[2] N. V Tkachenko, Z.-M. Sun, A.I, et al. Record Low Ionization Potentials of Alkali Metal Complexes with Crown Ethers and Cryptands, ChemPhysChem. 2019; 20: 2060–2062.

[3] D. V Konarev, S.S. Khasanov, M. Ishikawa, et al. Metallic conductivity versus charge disproportionation in C60 complexes with noninteger average charges on fullerene, ChemistrySelect. 2016; 1: 323–330.

[4] N. Maqsood, A. Asif, K. Ayub, et al. DFT study of alkali and alkaline earth metal-doped benzocryptand with remarkable NLO properties, RSC Adv. 2022; 12: 16029–16045.

[5] N. Kosar, L. Zari, K. Ayub, et al. NLO properties and electride characteristics of superalkalis doped all-cis-1,2,3,4,5,6-hexafluorocyclohexane complexes, Optik. 2022; 271: 170139.

[6] N. Kosar, L. Zari, K. Ayub,et al. Static, dynamic nonlinear optical (NLO) response and electride characteristics of superalkalis doped star like $C_6S_6Li_6$, Surfaces and Interfaces. 2022; 31: 102044.

[7] P. Das, P.K. Chattaraj, Comparison Between Electride Characteristics of $Li_3@B_{40}$ and $Li_3@C_{60}$, Front. Chem. 2021; 9: 638581